Measurements of CH_4, N_2O, CO, H_2O and O_3 in the Middle Atmosphere by the ATMOS Experiment on Spacelab 3

by

M. R. Gunson, C. B. Farmer, R. H. Norton,
Jet Propulsion Laboratory, Pasadena, CA 91109

R. Zander,
Universite de Liège, Liège, Belgium

C. P. Rinsland,
NASA Langley Research Center, Hampton, VA 23665

J. H. Shaw and Bo-Cai Gao,
Ohio State University, Columbus, OH 43210

Short Title: Minor Gases from ATMOS

Pages: 44
Tables: 4
Figures: 18

Submitted to Journal of Geophysical Research, February 1989.

ABSTRACT

The volume mixing ratios of five minor gases (CH_4, N_2O, CO, H_2O, and O_3) have been retrieved through the middle atmosphere from the analysis of 0.01 cm^{-1} resolution infrared solar occultation spectra recorded near 28°N and 48°S latitudes with the ATMOS (Atmospheric Trace Molecule Spectroscopy) instrument, flown on board Spacelab 3 (April 30 through May 6 1985). The results, which constitute the first simultaneous observations of continuous profiles through the middle atmosphere for these gases, are in general agreement with reported measurements from ground, balloon and satellite-based instruments for the same seasons. In detail, the vertical profiles of these gases show the effects of the upper and middle atmospheric transport patterns dominant during the season of these observations. The profiles inferred at different longitudes around 28°N suggest a near-uniform zonal distribution of these gases. Although based on fewer observations, the sunrise occultation measurements point to a larger variability in the vertical distribution of these gases at 48°S.

Measurements of CH_4, N_2O, CO, H_2O and O_3 in the Middle Atmosphere by the ATMOS Experiment on Spacelab 3

1. INTRODUCTION

The objective of the Atmospheric Trace Molecule Spectroscopy (ATMOS) experiment is the global investigation of the earth's upper atmosphere, based on measurements of the infrared solar spectrum recorded in the occultation mode from the space shuttle. The primary motivation for this work was to obtain a simultaneous inventory of the concentrations of the active atmospheric chemical species which influence the chemical and physical stability of the middle atmosphere. The first ATMOS flight took place when the instrument was included in the Spacelab 3 (SL-3) shuttle mission from April 30 to May 6 1985, and yielded about 500 high resolution, high signal-to-noise ratio spectra over a wide spectral region, covering tangent heights from 10 to 150 km. Analysis of these spectra has allowed us to include in this inventory most of the source, reservoir, and reactive trace gases important in the odd nitrogen, chlorine, and hydrogen chemical families of the middle atmosphere.

In this paper we present volume mixing ratio (vmr) profiles of five gases, CH_4, N_2O, CO, H_2O, and O_3, as a function of pressure and altitude in the middle atmosphere. The profiles of CH_4, N_2O, and H_2O cover the upper troposphere through to the mesosphere; the profiles of CO and O_3 extend from the upper troposphere to the lower thermosphere. The results from ATMOS sunset observations represent conditions at low northern mid-latitudes during the spring season; those inferred from sunrise occultations are appropriate to southern mid-latitudes in the fall. Differences between

sunset and sunrise results therefore reflect latitudinal, seasonal, and diurnal effects on the chemical composition and physical properties of the atmosphere.

The results presented here complete the initial findings on the simultaneous abundances of the chemical species determined from the ATMOS experiment's first flight. Details about the trace gases, including some first unambiguous detections, have already appeared in the literature (Toon et al., 1986; Zander et al., 1986; Park et al., 1986; Rinsland et al., 1986a,b), as have the inventories of the odd nitrogen family (Russell et al., 1988), the halogen source gases (Zander et al., 1987), and the halogen sinks and reservoirs (Raper et al., 1987).

It is interesting to note that a similar experiment, but utilising a Grille spectrometer rather than an interferometer to record infrared solar absorption spectra in occultation mode, was included in the Spacelab 1 (SL-1) shuttle mission from November 28 through December 8 1983 (see for example, Lemaitre et al., 1984). The measurements from this experiment are directly analogous to those made by the ATMOS instrument. The restricted spectral coverage and lower spectral resolution of the Grille spectrometer limited the number of atmospheric gases detected (Girard et al., 1988) but included some of those discussed in this paper in respect to ATMOS. Where appropriate the similarities and differences between these two space-borne spectroscopic investigations are noted below.

2. THE ATMOS SPACELAB 3 DATA BASE

An overview of the experiment can be found in Farmer and Raper (1986) and additional data on the instrument design and manufacture in Farmer et

al. (1987). In brief, the ATMOS instrument is a double-passed Michelson interferometer designed and built by Honeywell Electro-Optics Center in conjunction with the Jet Propulsion Laboratory. Solar occultation events occur very rapidly as seen from shuttle orbit (i.e., ~360 km altitude during the Spacelab 3 mission). In order to achieve good vertical resolution under these conditions, the ATMOS instrument records successive one million point double-sided interferogram every 2.2 secs. yielding a vertical spacing between spectra of about 4.2 km in the upper atmosphere. The vertical separations are reduced in the lower stratosphere and troposphere by refraction and by drift of the sun tracker field of view on the flattened solar disk. Each interferogram has a maximum optical path difference of 47.5 cm which, after transformation, produces an unapodized spectrum at ~0.01 cm^{-1} resolution. A cooled HgCdTe detector is used to provide coverage between 550 and 4800 cm^{-1}. In order to reduce the interferogram sampling rates and to improve the signal-to-noise ratio, the overall spectral response was divided into smaller, overlapping wavelength intervals using optical filters. Of the six available filters, three were designed for routine analysis for the concentration profiles of the minor gases (see Table 1).

Solar spectra were recorded by the ATMOS instrument during 19 occultation events, 12 sunsets and 7 sunrises. The location of the tangent points, the optical bandpasses, and the altitude coverage corresponding to the events used in this analysis of Spacelab 3 data are given in Table 1. All of the sunsets occurred between northern latitudes 25°N and 33°N and are identified by the letters SS followed by a number based on their

chronological order. The sunrise occultations occurred over the southern hemisphere between latitudes 47°S and 50°S; these are separately numbered and preceded by the letters SR.

After the interferograms were transformed at the JPL ATMOS Data Analysis Facility, the occultation spectra containing both solar, instrumental, and atmospheric spectral features were ratioed at each wavelength against the average of "pure solar" spectra (derived from 50 to 60 interferograms), obtained in the periods immediately before or after specific occultation events. This procedure eliminated instrumental as well as solar features, leaving only telluric absorptions in the spectra. Figure 1 shows an example of this procedure where a pure solar spectrum (Fig.1a) has been used with the raw unratioed spectrum (Fig.1b) to derive the atmospheric transmission spectrum (Fig.1c) used in the analysis. The resulting ratioed spectra germane to the present analysis were of the same high quality and have signal-to-noise ratios (estimated from the root mean square of the fluctuations in a non-absorbing region) of 300:1 in filter #1, 180:1 in filter #2, and 105:1 in filter #3 spectra. For the purposes of general display and analysis, the spectra have been apodized using one of the apodizing functions of Norton and Beer (1976). In Figure 1, the three spectra are plotted after convolution with the moderate strength apodizing function. Figure 2 shows a small region of the same three spectra, a "microwindow", which is typical of the size of regions chosen for analysis, and has been used in retrieving the H_2O vertical profiles. It shows clearly the presence of solar and residual instrumental H_2O absorption features.

Under high levels of incident photon flux, the ATMOS detector responded non-linearly to changes in the detected light levels, distorting recorded solar occultation interferograms. An empirical correction for this effect was determined and applied to interferograms recorded with optical filters #1 and #2. In uncorrected filter #3 spectra, the non-linearity of the detector was apparent as an offset of typically 2% in the zero transmission level. During the retrievals, the analyzed spectra were scaled to account for this. Its impact on the accuracy of the retrieved profiles is discussed below.

3. MOLECULAR SPECTRAL LINE PARAMETERS

The ATMOS SL-3 spectra have provided a unique opportunity to examine extensive regions of the infrared encompassing bands of the minor gases not normally recorded by other experiments. Any analysis of the data requires the best parameterization of the infrared features observed. For the analyses presented here, a separate compilation encompassing several hundred thousand lines has been formed, based on the AFGL 1982 line list (Rothman et al., 1983). It has been continuously updated and supplemented to reflect new measurements and calculations. An extensive discussion of this compilation (the "ATMOS Linelist") and of differences between it and other major listings (e. g. Rothman et al., 1987) has been given by Brown et al. (1987).

4. PRESSURE-TEMPERATURE MODELS

In the first phase of analysis of the ATMOS SL-3 data, physical properties of the atmosphere were retrieved, namely the vertical profiles of

pressure and temperature. This facet of the analysis allowed ATMOS to be a self-contained experiment which, apart from the molecular spectral line parameters, required little additional information from external sources for successful data reduction. This phase was carried out concurrently and iteratively with the retrievals of the concentration profiles of the minor and trace gases. The accuracies achieved in the temperature-pressure profiles ultimately establish the uncertainties associated with the mixing ratio profiles themselves (see later).

Four groups of coinvestigators associated with the experiment, i.e. those at the Jet Propulsion Laboratory, NASA Langley Research Center, Ohio State University, and Oxford University, developed independent methods to retrieve pressure-temperature profiles from the spectral data (Rinsland et al., 1987; Gao, 1988; Muggeridge, 1986). However, the philosophies and approaches adopted had much in common. The tangent point pressures were retrieved from the analysis of isolated spectral features of the "well known" constant volume mixing ratio gases, CO_2 and N_2, with spacings in altitude of successive scans derived initially from the mission ephemeris. Absorption lines selected for this purpose have well-determined line parameters, and have lower state energies that produce line intensities with minimal sensitivity to errors in the assumed temperature profile. In particular, the S-branch transitions of the N_2 1-0 electric quadrupole band around 2400 cm^{-1} provide a suitable means of estimating the tangent pressures from around 35 km down into the troposphere. CO_2 transitions of a number of vibration-rotation bands were used to provide tangent pressures from around 20 km up to 70 km.

The tangent point temperatures were estimated using isolated groups of lines in the R-branch of the CO_2 ν_3 fundamental band in the 2380-2394 cm^{-1} region. Transitions with the highest lower state energy, E", and hence largest J" value, have the greatest sensitivity to the tangent point temperatures. No other region was found with features which could provide comparable altitude coverage, temperature sensitivity, and the accuracy in line parameterization.

These measurements of temperature sensitive and temperature independent features provided the basis of the inversion methods coupled with the constraints imposed by hydrostatic and local thermodynamic equilibrium. At altitudes above 45 km, the height spacing of successive spectra approached a near constant value of 4.2 km at the tangent points. Below this height, the effects of refraction led to a steady reduction in spacing, further modified by the drift of the sun tracker field of view on the solar disk. Corrections for this effect were made by adjusting the heights of lower altitude scans to obtain optimum fitting of the temperature insensitive N_2 and CO_2 lines.

The temperature-pressure profiles retrieved from the sunset filter #3 occultations were found to be closely similar, leading us to adopt an average of these results to form a "zonal" physical model for use with all sunset occultations. These sunset occultations all fell within a narrow latitude band from 25° to 33°N. The reduced number of observations in the southern hemisphere rely on the physical model derived from a single sunrise occultation recorded with filter #3. The physical models were extended below 20 km and above 70 km using densities adopted from

climatological models. Approximate altitude scales corresponding to the northern and southern hemisphere physical models have been computed to facilitate comparisons with previously published profiles.

Estimates of the error contribution to the final mixing ratio profiles originating from the use of a mean zonal physical model and the determination of the viewing geometry are discussed below.

5. INVERSION METHODS

The retrieval of the volume mixing ratio profiles of the gases of interest then proceeded in a similar manner to that followed in deducing the atmospheric physical parameters. Several techniques were independently developed for these retrievals. Four of the methods relevant to the minor gas retrievals will be described in brief before comparing results from these methods and presenting the profiles for the minor gases.

The first of these schemes is a spectral fitting method which minimizes the weighted difference between observed and calculated spectral amplitudes. The retrieval as a function of altitude proceeds in an "onion-peeling" fashion, as described, for example, by Goldman and Saunders (1979). The program adjusts the target gas volume mixing ratio over specified, 1 km thick, atmospheric model layers until the observed spectral lines are fitted. Up to 150 layers, each homogeneous in pressure, temperature, and concentration, are included in this model of the atmosphere. The program operates in an interactive mode, with many additional parameters adjusted either manually or automatically. Following Russell et al. (1988), we will refer to this method as the "non-linear least squares difference"

(NLLD) scheme. In common with the other methods described below, the "best" results from this method were obtained by combining profiles inferred from many lines in narrow individual spectral regions, or "microwindows". These were selected to satisfy several criteria:

(i) the spectral intervals were relatively free from interfering absorption features of other telluric gases

(ii) the windows were selected with regard to using lines for which the spectroscopic parameters were best known

(iii) the windows contained transitions with lower state energies which gave the least sensitivity to uncertainties in the temperature profile.

As the number of molecules of the target gas along the line-of-sight varied by several orders of magnitude in one occultation, several microwindows were needed containing lines covering a corresponding range of line strengths. The microwindows used in this present work were contained within the spectral regions listed in Table 2.

The second scheme adopted a similar curve-fitting approach but based its criterion of fit on non-linear least squares (NLLS). The ATMOS implementation of this generic technique (Niple et al., 1980; Rinsland et al., 1982), uses 60 atmospheric layers, and can simultaneously retrieve the vmrs of 4 target gases while simulating 10 others. A number of instrumentral distortion effects, which can be adjusted automatically, or constrained to assumed values, have been included.

The third method uses measured equivalent widths and "onion-peeling" to infer a single target gas vmr profile. Typically, the equivalent

widths of five lines, each close to the linear part of the curve of growth (with maximum absorption depths of less than 30%, corresponding to an equivalent width of ~0.007 cm^{-1}), were measured from each spectrum and least-squares fitted to retrieve the mixing ratio at each tangent height (Rinsland et al., 1984). We refer to this as the "equivalent widths with onion-peeling" (EWOP) method.

The fourth method also used measured equivalent widths but introduced them into a non-linear least squares program. The volume mixing ratios were adjusted simultaneously at all altitudes until the best fit to measured equivalent widths was achieved (Gao, 1988). This procedure for inversion will be referred to as the "simultaneous fit of equivalent widths" (EWS) method.

A comparison of the results from these different techniques provides an insight into the precision of the retrieved profiles and the reliability of the retrieval schemes. The largest differences between test results from the algorithms described above were found to be ~5%. This figure has been taken to represent an estimate of the limiting accuracy of the retrieved profiles due to algorithm reliability. This will be demonstrated below for a typical case; in general, we have presented averaged profiles formed by combining results from the particular methods that were applied to individual occultation retrievals.

6. ERROR BUDGETS

The error budgets vary with species, altitude and the signal-to-noise (SNR) of the spectra. The following are the most significant factors that we have considered:

(i) uncertainties in observational geometry and validity of mean zonal physical models

(ii) retrieval algorithm accuracy

(iii) errors arising from the quality of the observed data

(iv) accuracy of the spectroscopic parameters

Each of these has been investigated in order to assess how its uncertainty impacts the accuracy of the retrieved profiles; they are discussed below (except algorithm accuracy which has been mentioned above) and summarized in Table 3. In this table, the error contributions have been separated into random (R) and systematic (S) errors appropriate to the retrieval of a vmr profile from an individual occultation using several microwindows.

Carbon dioxide plays an important role in the determination of the tangent heights and physical models of the atmosphere used in these analyses. A constant vmr of 330 ppmv was assumed for CO_2 at all heights up to 70 km. However, as a result of the secular increase in the CO_2 abundance and the reported difference between the tropospheric and stratospheric CO_2 vmr (World Meteorological Organisation, 1986) this may be in error by up to 10 ppmv; corresponding to a systematic error in inferred tangent pressures of no more than 4%. Furthermore, the magnitude of this uncertainty is reduced by the constraints imposed from a knowledge of the relative timing of individual spectra together with the mission ephemeris. We have estimated the systematic error in the tangent pressures to be 2%, with a corresponding error in the retrieved vmr.

Uncertainties in the CO_2 vmr profile also affect the accuracy of the inferred physical model temperatures, but these errors are minor because of the high sensitivity to temperature of the intensities of the high-J R-branch lines of the ν_3 band. Rinsland et al. (1989) have discussed briefly how the ATMOS zonal temperature profiles used in these analyses may differ from a "true" zonal profile, and estimated the largest fluctuations in the temperature profile over a spread of longitudes and latitudes by comparison to mean temperature measurements collected from 1979 to 1986 (Randel, 1987). They considered a temperature error of around 5 K; for the minor gases, and for lines selected having appropriate lower state energies to minimise the effect of this error source, this temperature error leads to a random error contribution of 1% in retrieved vmrs.

The uncertainty in the determination of tangent heights (or pressures) varies depending on the particular CO_2 bands used in the analysis which, in turn, depends on the optical filter used. The best determined are those for filter #2 spectra, which contain both useful CO_2 absorption features and have good SNR. In all the filters the precision with which the tangent heights were determined for spectra at heights below 40 km was better than for those with higher tangent heights. Typically, the tangent heights below 40 km were determined to better than ± 200 m in filter #2, corresponding to an error in vmr of 3%, and ± 300 m in filter #3, or an uncertainty of 5% in vmr. Although the spectra recorded with filter #1 have the best SNRs, the limited number of temperature insensitive CO_2 absorption features covering suitable altitude ranges limits the accuracy of the associated tangent heights to ± 500 m, or an uncertainty of 8% in

the retrieved vmr. The uncertainty in the viewing geometry, and the effect of this uncertainty on the derived physical parameters of the atmosphere, is the major limitation of the accuracy of vmr profiles inferred from filter #1 spectra.

Errors which define the spectral quality of the data have been divided into two components. The first is the effect of finite SNR, which improves with wavelength between the three filters considered. This random error source was reduced by combining retrievals from many, typically 10, spectral intervals. For a retrieval from a single feature in a filter #3 spectrum, having a SNR of 105:1, an excursion in spectral amplitude at line center equivalent to the RMS of the peak-to-peak noise produces as much as 10% change in the retrieved vmr. The better SNR in filters #1 and #2 greatly improved this sensitivity. An effective random error contribution from this source to the vmr value inferred from 10 microwindows, is included in Table 3.

The offset in the zero transmission level resulting from the non-linear response of the detector contributed significantly to the accuracy and precision of vmr profiles retrieved from filter #3. Corrections for the detector non-linearity applied to the interferograms obtained with filters #1 and #2, reduced these offsets to less than 0.5% of the total transmission. In uncorrected filter #3 spectra these offsets were typically ± 2%, growing to 5% at the filter edges. The offsets in the zero level were observed to vary slowly with wavelength and, to a lesser extent, with tangent height of the spectra. Where a residual offset could be measured from opaque regions of spectra at lower altitudes, a rescaling of

the spectra at all altitudes was made at the wavelengths of interest. This procedure reduced the uncertainty in the zero transmission in filter #3 spectra to ± 1%. The random and systematic error components in Table 3 have been included to account for the sensitivity of the retrieved vmr to zero level offsets.

A common characteristic of the gases considered in this paper is the relatively high accuracy in their associated spectroscopic parameters. Errors in the line strengths and air-broadening parameters propagate directly to errors in the retrieved vmrs. The line strength parameters are in general accurate to about 5%, except O_3 which has been put at 10%. Evidence of the quality of these parameters, given the high precision with which the observational data were fitted, can be seen in the good agreement between vmr-height profiles inferred from different vibrational bands.

The air broadened line widths of the gases considered in this paper are some of the best known, with accuracies of better than 10%. Accurate line broadening parameters are most important to the retrievals of the minor gases from spectra with tangent heights below 25 km. In this altitude range, uncertainties in the broadening parameter of 10% introduce errors of less than 5% in vmr. Uncertainties in the other spectroscopic line parameters have less impact on the accuracy of vmr retrievals and can be ignored in this discussion.

In Table 3 the exemplar total random and systematic errors have been computed as the root-sum-square (RSS) of the various components. The precision associated with a profile retrieved from a single occultation has been determined from the variance of the mean of the vmrs inferred from

several microwindows. The reciprocal squares of the precisions have been used to weight the data in forming zonal mean profiles from the more numerous sunset occultations. However, for the limited number of sunrise measurements a simple average of available results was made with the precision computed as the RSS of those of the individual occultation profiles. The accuracy of the zonal profiles was then computed as the sum of the precision and the total systematic error given in Table 3. These have been employed in subsequent figures and tables showing 1σ error bars for the total uncertainty.

7. RETRIEVAL RESULTS

Methane

Spectral signatures for methane were observed in ATMOS spectra up to 65 km in altitude. In this analysis, lines from the ν_2 and ν_4 bands which occur in filter #2 spectra, and lines of the $2\nu_4$, $\nu_2+\nu_4$, and ν_3 bands (Table 2) which occur in the filter #3 spectra, have been used to infer the volume mixing ratio-height profiles of $^{12}CH_4$. This molecule provides a useful example of the results obtained by different retrieval methods as the accuracies of the spectral line parameters for these bands are thought to be particularly good (Brown et al., 1987), thus eliminating spectroscopy as a major source of error.

Figure 3 presents a typical fit by the NLLD method for a microwindow containing three CH_4 lines used for retrievals at high altitudes (30 - 65 km). The residuals of the fit are close to the noise level of the data, indicating the good precision obtained with such schemes.

The SS07 occultation retrieval results derived using four different retrieval methods are presented in Fig. 4. The profiles agree well with one another within the estimated standard deviations. The 1σ error bars for only one profile are plotted and are representative of the precision associated with the vmr values retrieved from different schemes; for CH_4 these have typical values of 5-10%.

Some days later (May 10, 1985) and close to the location of the ATMOS SL-3 SS07 occultation, the Université de Liège grating spectrometer recorded infrared solar absorption spectra during a balloon flight from Palestine, Texas (flight ULG-20). CH_4 column amounts measured from these spectra agreed with those determined from the ATMOS SS07 CH_4 profile to within 4% (R. Zander, private communication).

Profiles inferred from all of the filter #2 and #3 sunset occultations, using the NLLD method, are presented in Fig. 5. This is intended to show the overall consistency among the individual results. These have been used to form a mean zonal profile (Fig. 6) representative of the 25° to 33°N latitudes sampled by ATMOS.

Southern hemisphere CH_4 vmr profiles were inferred from two sunrise occultation events, one each with filters #2 and #3. The mean of the two profiles is also plotted in Fig. 6 for comparison with the mean zonal profile formed from the sunset occultation results. The notable features of, and differences between, the two hemispheres are discussed below in reference to the measurements of the N_2O vertical distributions.

Nitrous oxide

Like methane, the N_2O infrared bands between 3 and 10 μm are considered

to be among the best in terms of the accuracies associated with the spectroscopic line parameters. The profiles retrieved from the sunset filter #2 and #3 occultations are plotted in Fig. 7. The mean sunset and sunrise N_2O profiles are plotted in Fig. 8, with 1σ error bars indicating the estimated accuracy of the mean. These results are also given in Table 4. The marked contrast in profiles is discussed below.

Comparison of Methane and Nitrous Oxide Profiles

The accuracy and validity of the present results for CH_4 and N_2O (and to some extent the validity of the profiles subsequently presented) can be determined by a comparison with other observations of these gases and current models of atmospheric behaviour. In the ATMOS pre-flight planning, typical mid-latitude vmr-height profiles for these gases were constructed to reflect this knowledge. The sources of both CH_4 and N_2O are at the surface and, as a result of their long tropospheric lifetimes, they are relatively well mixed and uniformly distributed up to heights of ~15 km. In the stratosphere their relative concentrations decrease with height due to photochemical destruction. This lapse rate has been observed to be lower at equatorial latitudes where the increased upwelling of tropospheric air through diabatic heating mitigates against photochemical losses (World Meteorological Organisation, 1986). This "first order" description leads to height profiles with a constant vmr in the troposphere and a monotonically decreasing vmr above 20 km. Observational evidence for this can be found, for example, in the vertical distributions of CH_4 and N_2O measured by the Grille spectrometer experiment during the Spacelab 1 space shuttle mission at northern mid-latitudes and southern high latitudes

(Muller at al., 1985; Girard et al., 1988).

The inferred profiles from the ATMOS sunrise occultations, taken around 48°S (i.e. the fall hemisphere), also follow the simple description given above. At tropospheric and low stratospheric altitudes, the profiles are consistent with accepted surface values, followed by a rapid but monotonic decrease in vmr in the upper stratosphere. In contrast to this, however, mean zonal profiles for 28°N show a "fold" or layer of near constant vmr at at heights between 30 and 40 km.

Results from the SAMS (Stratospheric and Mesospheric Sounder) instrument flown on the NIMBUS 7 satellite (Jones, 1984) have provided the basis of much of the current understanding of the global stratospheric distribution of these two gases. Given the confidence associated with these SAMS measurements it is pertinent to examine the reported results for similar features. The measurements made by SAMS over a three year period revealed several interesting phenomena. These included the appearance of a "double peak" in the latitudinal distribution of these gases about the equator in the northern hemisphere spring season (Jones and Pyle, 1984). Gray and Pyle (1986, 1987), in a two-dimensional model study, have shown that the main features of the "double peak" could be reproduced by including the forcing of the semi-annual oscillation. A second, dynamical, explanation was put forward by Solomon and Garcia (1984), and later by Solomon et al. (1986), in which the double peak in CH_4 was reproduced in a model study by including transport through the diabatic circulation. The folds appearing in the ATMOS profiles may be a consequence of the same physical processes which produced the double-peak. There is some evidence of altitude ranges of constant mixing ratio within the SAMS CH_4 monthly mean distributions presented by Jones and

Pyle, but at the same latitudes, heights and month, there appear to be no similar features in the N_2O distributions. The lack of a conclusive correlation between these two tracers is not surprising given the poorer vertical and temporal resolution, or the uncertainties associated with the SAMS measurements.

Ehhalt and Tonniben (1979) have commented that similarly perturbed profiles are not an uncommon observation at low mid-latitudes nor are they confined to any particular season. This was based on a review of a large number of rocket- and balloon-borne in-situ cryo-sampler measurements of these gases made by various experimenters. The regions of near-constant mixing ratio in the stratosphere generally occurred at the upper altitude limit of the balloon-borne measurements, whereas the present results are possibly the first to show the vertical extent of this feature and the return to the steady decrease in vmr with height above 40 km.

These authors pointed out that phenomena of this kind can be explained as a consequence of the stratospheric Hadley circulation. A quasi-horizontal motion in the meridional plane, and in a poleward direction, occurs when the Hadley cell displaces air from the tropical mid-stratosphere into the lower stratosphere at mid-latitudes. If the tropical air maintains its characteristic of a weaker vertical gradient then a fold is created in the vmr profiles at mid-latitudes.

More recently, Offermann et al. (1987) reported a similar structure in the vmr-height profiles of several stratospheric trace constituents observed during the MAP/GLOBUS 1983 campaign. These measurements, which were made in Southern France (44°N), were spread over a 1 month period

between September and October of that year. The results for a total of 14 trace gases showed "wavelike disturbances". The profiles for CH_4, N_2O, and CF_2Cl_2 measured by two in-situ cryo-samplers (Schmidt et al., 1987) show the lower portions of folds in the vmr-height profiles similar to the present ATMOS SL-3 results. A comparison between the ATMOS and MAP/GLOBUS CCl_2F_2 profiles was less revealing since the region of near constant mixing ratio lies above the highest altitude (30 km) at which CF_2Cl_2 was detected by ATMOS (Zander at al., 1987). The remaining minor gases, including those discussed in this paper, are less sensitive tracers of this process due to the general shape of their unperturbed vmr-height profiles and the weaker gradients in their meridional distribution. Offermann et al. concluded that the wavelike disturbance observed in the MAP/GLOBUS campaign had a horizontal scale of the order of 1300 km and a time scale of 10 days. They also suggested vertical transport through a slantwise convection of air parcels as the principle dynamical source of the wavelike structures, discarding a larger meridional, quasi-horizontal transport as being too weak to be the cause. The close agreement between separate ATMOS observations of CH_4 and N_2O at several longitudes within the 28°N latitude band indicate a zonally uniform distribution and hence a large east-west horizontal scale for this phenomenon. Indeed, at these lower mid-latitudes a single standing wave may account for these observations, while at the higher latitudes of the MAP/GLOBUS measurements, in the "surf zone" as described by MacIntyre and Palmer (1984), the wave structure could have a much higher wavenumber. A better understanding of this perturbation needs further investigation and modelling.

Carbon monoxide.

The 1-0 band of CO around 2050-2200 cm^{-1} is observed only in the filter #3 bandpass. Features of this band were detected in all spectra corresponding to tangent heights between 10 and 105 km. The profile values inferred from the four filter #3 sunset occultations are plotted in Fig. 9. Carbon monoxide has natural and anthropogenic sources in the troposphere; in the thermosphere it is produced by photodissociation of CO_2. These sources are reflected in the near constant mixing ratios at the two altitude extremes of the retrieved profiles both at sunset and sunrise (Fig. 10). In the stratosphere and mesosphere, the dominating photochemical process by the loss of CO through its reaction with OH to form CO_2, is set against the production of CO principally from the oxidation of CH_4. The CO photochemical lifetime at these altitudes is longer than the time scale of dynamical events, and it can be used as a tracer through these regions (Allen et al., 1981; Solomon et al., 1985).

The distinctive north-south CO profile differences observed here can be qualitatively explained with a simple Brewer-Dobson circulation model for the upper stratosphere and mesosphere. This requires a single summer-hemisphere-hemisphere-to-winter-pole (in this instance southward) circulation cell to produce an increase in the downward flux of CO-rich air at southern latitudes. The same trends appear in the CO vertical profiles inferred from the measurements of the Grille spectrometer on SL-1 (Vercheval et al., 1986; Girard et al., 1988). In these observations the northern mid-latitude measurements correspond to the winter hemisphere and show an increased CO abundance in the mesosphere over those measured at southern latitudes,

consistent with the circulation described above.

At high altitudes the monochromatic absorptance and the equivalent widths of lines of atmospheric gases are very non-linear in their dependance on the amount of absorber. This greatly reduces the precision of retrieved values of vmr at these heights. This is particularly true for CO, and is reflected in the uncertainties or estimated standard deviations of the vmr profiles given in Table 4. This uncertainty is largest in an onion-peeling retrieval for CO where, at stratospheric altitudes, a significant portion of the absorber lies at higher levels than those being analyzed. Thus the largest percentage uncertainties are associated with CO volume mixing ratios inferred between 30 and 85 km.

Water Vapor

The 1982-83 balloon intercomparison campaigns (BIC 1 and 2) of stratospheric water vapor measurements (Murcray et al., in press) were directed at understanding the inconsistencies in results between various experimental methods. This stemmed from the concern that the wide range or apparent variability observed in H_2O was not natural but had its origin in instrumental errors. Despite the high precision obtained by various techniques, measurements made from balloon platforms must discriminate between atmospheric H_2O and large amounts of H_2O outgassing from the balloon and instrument. Remote sensing measurements made from space offer distinct advantages in this respect: the background instrumental and platform H_2O is significantly reduced, and the Doppler shift resulting from the relative velocity between the earth's atmosphere and the spacecraft greatly aids in discriminating between the sources of the spectral signals.

In the ATMOS spectra, residual instrumental H_2O absorption lines were clearly shifted from the atmospheric absorptions (by ~0.03 cm^{-1} at 1500 cm^{-1}, from a velocity difference of >6 km s^{-1}) and could be removed by ratioing spectra containing the telluric absorption features of interest against pure solar spectra (see Figs. 1 and 2). An absorption versus emission measurement technique offers a further advantage in that it minimizes the error due to uncertainties in the atmospheric temperature profile and its effect on atmospheric emissivity. Thus a space-borne absorption spectrometer provides an opportunity to make accurate measurements of atmospheric water vapor by reducing the problems inherent in other techniques.

Retrievals of water vapor abundance were made in filter #2 and #3 occultations using H_2O^{16} absorption lines in the ν_2 (6.2 μm) band and to a lesser extent the $2\nu_2$ (2.7 μm) band. The strongest lines of the ν_2 band were discerned in spectra with nominal tangent heights as high as 90-92 km, and up to 75 km in the $2\nu_2$ region.

Individual lines in more than 50 microwindows were used to give complete altitude coverage from the tropopause to the thermosphere. The present analyses were based on the line parameters for the ν_2 band appearing in the AFGL HITRAN 1982 compilation (Rothman et al., 1983). Table 2 lists the altitude coverage provided by these lines, grouped by line strengths, together with an estimate of the group line strength accuracy. Absorptions due to isotopic variants of water have been observed in the ATMOS spectra and will be reported separately.

The individual sunset profiles retrieved by the NLLD method are plotted

in Fig. 11, and the two sunrise observations in Fig. 12. The better agreement among the sunset profiles has led us to form a representative 28°N zonal profile from the weighted average of these individual observations. The larger differences between the sunrise measurements of H_2O are an indication of the zonal variability of the atmosphere to be expected at higher latitudes. It would be more appropriate in such circumstances to form a true zonal H_2O profile from a larger and more representative sample. However, for consistency with our previous practice we have taken the mean of the two profiles and estimated the uncertainty as the root-sum-square of the individual profile uncertainties. This has been included in Table 4 along with the sunset mean profile.

In the northern hemisphere, the minimum in the ATMOS H_2O mixing ratio profile at the tropopause is very pronounced; above this there is a steady increase in H_2O up to 60 km where it reaches a maximum of 6.6 ppmv. Contrary to these findings, Remsberg et al. (1984) comment that in general the measurements by the Limb Infrared Monitor of the Stratosphere (LIMS) show a near-constant vmr of 5 ppmv through the upper stratosphere. However, they present a LIMS mean H_2O profile for 32°N in May which agrees remarkably well with these present results (Fig. 13). Included in this figure are ground-based microwave H_2O measurements made at JPL in Pasadena, California (34°N), around May 1, 1985 (Bevilacqua et al., 1987). These authors show values with a range of ± 0.5 ppmv about those plotted for this period. Both sets of measurements reproduce a rapid fall off in H_2O above 60 km. Two low mid-latitude H_2O profiles, measured by the Grille spectrometer on SL-1 (Girard et al., 1988), are plotted in Fig. 13 for

comparison. The profiles correspond to occultations at 31°N and 24°N (events 13 and 21 respectively) during the late fall when the SL-1 mission took place. These measurements show systematically lower H_2O in the stratosphere than either ATMOS or LIMS, with a minimum of 1.7-1.9 ppmv at 30 km rising to 4.7-5.0 ppmv at 55 km.

The tropopause and hygropause in the southern, and in this instance fall, hemisphere occur at lower altitudes. This is reflected in the retrieved H_2O profile from the occultation SR05 which shows no minimum in the volume mixing ratio at these altitudes, although there is some slight evidence of such a minimum in the SR02 retrieved profile (Fig. 12).

Total Hydrogen

The total hydrogen at any altitude in the stratosphere is related to the sum of H_2O and CH_4. Thus, in the absence of any other source, the vertical gradient in the water vapor profile can be correlated with the destruction of methane by a simple conservation law

$$\text{Total hydrogen} = H_2O + 2*CH_4 + (\text{H-species})$$

where (H-species) represents all other hydrogen containing species (though principally H_2 itself at stratospheric altitudes). The last term can be deemed constant at around 0.5 ppmv and the sum of water and methane alone considered (Pollock et al., 1980; Rinsland et al., 1984; Jones et al., 1986). Ellsaeser (1983) proposed that any increase in water vapor not accounted for by methane oxidation should be considered to be solely due to the limitations of instrumental accuracy.

Jones at al. (1986) evaluated this expression for the hydrogen budget using data for CH_4 and H_2O from the NIMBUS 7 SAMS and LIMS instruments over a range of latitudes and altitudes and concluded that this conservation law is in general obeyed.

The ATMOS data are particularly well suited to this test since the volume mixing ratio profiles are obtained simultaneously with one instrument and with a precision better suited to a test of this hypothesis. In Fig. 14 we present the sum of the mean sunset zonal profiles of methane and water vapor, weighted to give total hydrogen. Within the estimated uncertainties, the sum of H_2O and CH_4 as defined above remains constant at a value ~7.0 ppmv. However, the best fit to the sunset profile is achieved while allowing for an increase in total hydrogen with altitude of 6.95 ppmv at 30 km to 7.39 ppmv at 50 km. Part of this increase can be offset by including model H_2 profiles (Ehhalt and Tonniben, 1979; L. Froidevaux private communication) into the summation, which show H_2 decreasing with altitude through oxidation by O ^1D. The minimum in these H_2 profiles occurs between 40-60 km and corresponds to 0.25 ppmv of H_2O; still somewhat less than the 0.4 ppmv difference in total H_2 shown above. Bevilacqua et al. (1983) interpreted ground-based microwave measurements of maximum H_2O vmrs at 55 and 60 km as the result of diffusion creating a small net flux of water vapor into the stratosphere from a source region in the lower mesosphere. Similar studies by Remsberg et al. (1984) of the LIMS H_2O measurements showed regions and altitudes where the increase in H_2O could not be explained by methane oxidation alone, and suggested that transport should be considered to play a role. Indeed, the southern hemisphere measurements of H_2O and CH_4

derived from the SR05 and SR06 occultation events tend to confirm this conclusion. Large differences in H_2O were measured between these occultations, but with no corresponding changes in CH_4 to maintain a constant value in total H_2 with altitude. The magnitude of the additional source of H_2O requires further studies, both to improve the accuracy of measured profiles and in the understanding of the chemical and physical processes involved in the stratospheric H_2O budget.

Ozone

The O_3 fundamental ν_3 band at 9.6 μm was observed in both filter #1 and #2 occultation spectra up to heights of 100 km. Additional features in several other weaker bands were detected below 60 km, including the ν_1 fundamental and the $\nu_1+\nu_2$, and $\nu_2+\nu_3$ combination bands at 5.7 μm in filter #2 spectra; and the $\nu_1+\nu_3$ combination band at 4.7 μm in filter #3. The uncertainties associated with O_3 line strengths in different bands are the largest among the gases considered here. The original parameters used in analyzing this present data are described by Brown et al. (1987). They include line parameters for the ν_1 and ν_3 bands derived from an analysis by Pickett et al. (1985); these are also found in the latest edition of the AFGL HITRAN linelist (Rothman et al., 1987). A recent reanalysis of these bands by Flaud et al. (1987) has extended the range of transitions studied both in measured line positions and relative line strengths. New values for the line positions and strengths were calculated which included some significant changes in the relative strengths of transitions used in the present retrievals. These new values have been used to infer the vmr-height profiles reported here. Justification for this selection of line

parameters was made with consideration to the larger experimental data base employed in their derivation, together with the better agreement achieved between profiles inferred from different O_3 bands in the ATMOS spectral bandpass. A more detailed discussion is included below.

Ozone is the only molecular species of those considered here which is expected to exhibit a significant diurnal variation in concentration. The largest changes in concentration occur at dusk and dawn while new photochemical equilibria are established (Allen et al., 1984). The distribution of O_3 about the tangent point is determined by the variation of O_3 abundance with height and solar zenith angle. Model calculations using the Caltech 1-D photochemical model (Allen et al., 1984; Froidevaux et al., 1985) indicate that the asymmetry in O_3 distribution about the tangent point should be largest at sunrise near 70 km. Boughner et al. (1980) described a method to account for this asymmetry in retrieval processes. This methodology was applied to the ATMOS analysis (L. Froidevaux, private communication, 1986), as mentioned also for the NO and NO2 profile retrievals (Russell et al., 1988), by including model correction factors to account for the change in O_3 (relative to the tangent point abundance) along the ray path. Such a correction is needed in the mesosphere, particularly between 60 and 85 km, where the asymmetry is strongest; differences between corrected and uncorrected retrievals were found to exceed 40% near 70 km for the sunrise cases, but not moer than 6% near 60 km for sunset events.

The O_3 profiles inferred from the sunset and sunrise occultations are shown, respectively, in Figs. 15 and 16. These profiles were retrieved from O_3 features in the 9.6 μm region using the NLLD curve fitting algorithm

(ozone infrared bands are poorly suited to retrieval schemes based on measured equivalent widths as they are characterized by a high spectral density of rovibrational transitions). The notable differences in the two sets of profiles result from a combination of latitudinal and diurnal variations. Below 35 km the ozone abundance is controlled by dynamical processes and the differences in the profiles are representative of latitudinal variations determined by the seasonal circulation patterns. Above this altitude, the ozone abundance is controlled by faster photochemical processes which, in turn, depend on the atmospheric composition, temperature and the solar flux. At mesospheric altitudes, sunrise-sunset differences reflect the effects of the diurnal variation mentioned above. Between 70 and 80 km the sunrise O_3 vmr values represent an upper limit determination from SR06 occultation spectra. In these cases, the O_3 vmr in target layers was increased until a perceptable change occurred in the residual differences between observed and calculated spectra.

During the period of observation of the atmosphere by ATMOS, the SAGE II instrument was successfully operating on the Earth Radiation Budget satellite (Mauldin et al., 1985). This experiment also operates in a limb-viewing, solar occulatation mode, but uses visible absorption bands to measure the aerosol content and the abundance of several gases in the middle atmosphere. Measurements of O_3 by this instrument were made around 28°N and 48°S, at sunset and sunrise respectively, two or three days before the ATMOS observations. The range in O_3 vmr values derived from over 40 SAGE II occultations (M. P. McCormick, unpublished data) at these latitudes are presented in Fig. 17 as the shaded regions for

comparison with the present results.

At both latitudes, the ATMOS and SAGE II results show remarkable agreement in the shape of the O_3 vertical profiles. However, the range in SAGE II measurements indicate a large longitudinal variability around 48°S in a dynamically active region. The larger differences already noted above in the retrieved ATMOS sunrise H_2O profiles may be a result of this same activity.

The bandpasses of the ATMOS optical filters each encompass several vibrational bands of O_3. This present data set has provided an opportunity, not often available in the laboratory, to examine the relative accuracies of the spectroscopic parameters of these bands. Indeed, in the course of the analysis of the data it became apparent that currently the largest source of systematic errors associated with the retrieved O_3 vmr profiles lies in the spectroscopic parameters.

In the ATMOS filter #2 and filter #3 spectra, at heights below 55 km, several overtone and combination bands have been observed in addition to the fundamental bands at 9.6 μm. Profiles retrieved from filter #2 and #3 sunset occultations are plotted in Fig. 18. These profiles were based on lines taken from three spectral regions: at 9.6 μm (ν_1 band), 5.7 μm (the $\nu_1+\nu_2$, $\nu_2+\nu_3$ bands), and 4.7 μm ($\nu_1+\nu_3$ band). Profiles inferred with line parameters from two different studies, that of Pickett et al. (1985) and Flaud et al. (1987) of the 9.6 μm band, are included. The principal difference between these two studies lies in the line strengths associated with the weaker ν_1 band, although the values for the stronger ν_3 band are in relative agreement. Profiles inferred from the shorter wavelength

bands (5.7 and 4.7 μm) and those retrieved using the 9.6 $\mu m \nu_1$ band line parameters of Flaud et al. (1987) agree quite closely. These profiles are also in good agreement with the measurements made by the SAGE II experiment using O_3 bands in the visible region. This strongly suggests that the relative line strengths derived from the analysis of Flaud et al. (1987) should be adopted for the O_3 ν_1 and ν_3 fundamental bands.

8. CONCLUSION

The simultaneous measurement of several minor gases through the middle atmosphere by the ATMOS instrument has provided evidence of the effects of the dynamical processes and circulation patterns dominant at the northern spring/summer and southern fall/winter seasons. The vertical profiles of CH_4 and N_2O reported here, based on observations at several longitudes around 30°N, are consistent with an equator-to-low latitude circulation cell in the northern hemisphere. The present measurements also show an enhancement of CO in the southern mesosphere, coinciding with the downward limb of a summer-to-winter hemisphere circulation cell at these altitudes. The effects of this circulation pattern, but for the opposite season, was observed in the CO mesurements from the Spacelab 1 grille spectrometer experiment (Girard et al. 1988).

Little variation was found in vmr-height profiles of the minor gases inferred from occultations in the lower northern mid-latitudes (28°N). This zonal stability was not reproduced in the profiles determined from the limited number of observations in the southern hemisphere at high mid-latitudes. In particular, the range in mesopheric volume mixing ratios of O_3 and H_2O inferred for 48°S, suggests a significant variability

variability in their abundance, perhaps as a consequence of wave activity in this region. It is evident that more extensive seasonal and spatial coverage of data of this quality would be of value in validating the dynamical component of sophisticated atmospheric models.

This present study shows an increase with altitude, from the tropopause through the stratosphere, in the H_2O volume mixing ratio which is in excess of the reduction in CH_4 by oxidation over the same altitudes. This is being investigated further to eliminate and minimize experimental uncertainties, but within the precision of these measurements this observation is at odds with a simple view of the H_2-budget in the stratosphere.

The ATMOS O_3 profiles inferred from the 9.6 μm spectral region are in good agreement with the measurements obtained by the SAGE II satellite instrument. A comparison of O_3 profiles retrieved from several bands, and based on line parameters generated from separate analyses, has pointed to a large area of work where laboratory and atmospheric spectra of this quality can be combined to increase the scope and accuracy of the spectroscopic data base.

Acknowledgements

This research was performed at the Jet Propulsion Laboratory, California Institute of Technology, under contract to the National Aeronautics and Space Administration. Acknowledgement is made to L. Brown, L. Lowes, S. Paradise and R. Toth for their support and comments during this work, to M. Allen and L. Froidevaux for helpful discussions, to M. P. McCormick and R. Vega for providing SAGE II O_3 profiles prior to publication, and to Juock Namkung for her assistance in clarifying apparent differences in retrieval schemes.

References.

Allen, M., Y. L. Yung and J. W. Waters, "Vertical transport and photochemistry in the terrestrial mesosphere and lower thermosphere (50-120 km)," J. Geophys. Res., 86, 3617 - 3627, 1981.

Allen, M., J. I. Lunine and Y. L. Yung, "The vertical distribution of ozone in the mesosphere and lower thermosphere," J. Geophys. Res., 89, 4841 - 4872, 1984.

Bevilacqua, R. M., J. J. Olivero, P. R. Schwartz, C. J. Gibbins, J. M. Bologna and D. L. Thacker, "Observational study of water vapor in the mid-latitude mesosphere using ground-based microwave techniques," J. Geophys. Res., 88, 8523 - 8534, 1983.

Bevilacqua, R. M., W. J. Wilson and P. R. Schwartz, "Measurements of mesospheric water vapor in 1984 and 1985: results and implications for middle atmospheric transport," J. Geophys. Res., 92, 6679 - 6690, 1987.

Boughner, R. E., J. C. Larsen and M. Natarajan, "The influence of NO and ClO varaitions at twilight on the interpretation of solar occultation measure-ements," Geophys. Res. Lett., 7, 231 - 234, 1980.

Brown, L. R., C. B. Farmer, C. P. Rinsland and R. A. Toth, "Molecular line parameters for the Atmospheric Trace Molecule Spectroscopy (ATMOS) experiment," Appl. Opt., 26, 5154 - 5182, 1987.

Ehhalt, D. H. and A. Tonniben, "Hydrogen and carbon compounds in the strato-sphere," Proceedings of the NATO Advanced Study Institute on Atmospheric Ozone: Its variation and human influence, Report No. FAA-EE-80-20, 129 - 151, 1979.

Ellsaesser, H. W., "Stratospheric water vapor," J. Geophys. Res., 88, 3897 - 3906, 1983.

Farmer, C. B. and O. F. Raper, "High resolution spectroscopy from space: a preliminary report on the results of the Atmospheric Trace Molecule Spectroscopy (ATMOS) experiment on Spacelab 3," NASA Conference Proceedings, CP-2429, 1986.

Farmer, C. B., O. F. Raper and F. G. O'Callaghan, "Final report on the first flight of the ATMOS instrument during the Spacelab 3 mission, April 29 through May 6, 1985," Jet Propulsion Laboratory Publication 87-32, 1987.

Flaud, J.-M., C. Camy-Peyret, V. Malathi Devi, C. P. Rinsland and M. A. H. Smith, "The ν_1 and ν_3 bands of $16O_3$: line positions and intensities," J. Mol. Spectrosc., 124, 209 - 217, (1987).

Froidevaux, L., M. Allen and Y. L. Yung, "A critical analysis of ClO and O_3 in the mid-latitude stratosphere," J. Geophys. Res., 90, 12999 - 13030, 1985.

Gao, B. C., "The retrieval of atmospheric temperatures and gas volume mixing ratios and column amounts from infrared solar absorption spectra," Cooperative Thesis No. 113, The Ohio State University and National Center for Atmospheric Research, 1988.

Girard, A., J. Besson, D. Brard, J. Laurent, M. P. Lemaitre, C. Lippens, C. Muller, J. Vercheval and M. Ackerman, "Global results of the grille spectrometer experiment on board Spacelab 1," Planet. Space Sci., 36, 291 - 300, (1988).

Goldman, A. and R. S. Saunders, "Analysis of atmospheric infrared spectra for altitude distribution of atmospheric trace constituents. I. Method of analysis," J. Quant. Spectrosc. Radiat. Transfer, 21, 155 - 161, 1979.

Gray, L. J. and J. A. Pyle, "Semi-annual oscillation and equatorial tracer distributions," Quart. J. Roy. Meteorol. Soc., 112, 387 - 407, 1986.

Gray, L. J. and J. A. Pyle, "Two-dimensional studies of equatorial dynamics and tracer distributions," Q. J. R. Meteorol. Soc., 113, 635 - 651, 1987.

Jones, R. L., "Satellite measurements of atmospheric composition: Three years' observation of CH_4 and N_2O," Adv. Space Res., 4, 121-130, 1984.

Jones, R. L. and J. A. Pyle, "Observations of CH_4 and N_2O by the NIMBUS 7 SAMS: A comparison with in situ data and two-dimensional numerical model calculations," J. Geophys. Res., 89, 5263 - 5279, 1984.

Jones, R. L., J. A. Pyle, J. E. Harries, A. M. Zavody, J. M. Russell III and J. C. Gille, "The water vapour budget of the stratosphere studied using LIMS and SAMS satellite data," Quart. J. Roy. Meteorol. Soc., 112, 1127 - 1143, 1986.

Lemaitre, M.-P., J. Laurent, J. Besson, A. Girard, C. Lippens, C. Muller, J. Vercheval and M. Ackerman, "Sample performance of the Grille spectrometer," Science, 225, 171 - 172, 1984.

Mauldin III, L. E., M. P. McCormick Jr., L. R. McMaster and W. R. Vaughan, "The stratospheric aerosol and gas experiment II (SAGE II) design and in-orbit performance," SPIE, 589, 104 - 111, 1985.

McIntyre, M. E. and T. N. Palmer, "The 'surf zone' in the stratosphere," J. Atmos. Terr. Phys., 46, 835 - 849, 1984.

Muggeridge, A. H., "The retrieval of atmospheric pressure and temperature profiles from high resolution absorption spectra", D. Phil. Thesis, Oxford University, 1986.

Muller, C., J. Vercheval, M. Ackerman, C. Lippens, J. Laurent, M. P. Lemaitre, J. Besson and A. Girard, "Observations of middle atmospheric CH_4 and N_2O vertical distributions by the Spacelab 1 grille spectrometer," Geophys. Res. Lett., 12, 667 - 670, (1985b).

Murcray, D. G., A. Goldman, J. Kosters, R. Zander, W. Evans, N. Louisnard, C. Alamichel, M. Bangham, S. Pollitt, B. Carli, B. Dinelli, S. Piccioli, A. Volboni, W. Traub, and K. Chance, "Intercomparison of stratospheric water vapor profiles obtained during the balloon intercomparison campaign," J. Atmos. Chem., (in press, 1988).

Niple, E., W. G. Mankin, A. Goldman, D. G. Murcray and F. J. Murcray, "Stratospheric NO_2 and H_2O profiles from high resolution infrared solar spectra using nonlinear least squares," Geophys. Res. Lett., 7, 489 - 492, 1980.

Norton, R. H. and R. Beer, "New apodizing functions for Fourier spectrometry," J. Opt. Soc. Am., 66, 259 - 264, 1976.

Offermann, D. and others, "Disturbance of the stratospheric trace gas mixing ratios during the MAP/GLOBUS 1983 campaign," Planet. Space Sci., 35, 673 - 684, 1987.

Park, J. H., R. Zander, C. B. Farmer, C. P. Rinsland, J. M. Russell III, R. H. Norton and O. F. Raper, "Spectroscopic detection of CH_3Cl in the upper troposphere and lower stratosphere," Geophys. Res. Letts., 13, 765 - 768, 1986.

Pickett, H. M., E. A. Cohen and J. S. Margolis, "The infrared and microwave spectra of ozone for the (0,0,0), (1,0,0) and (0,0,1) states," J. Mol. Spectrosc., 110, 186 - 214, 1985.

Pollock, W., L. E. Heidt, R. Lueb and D. H. Ehhalt, "Measurements of stratospheric water vapor by cryogenic collection," J. Geophys. Res., 85, 5555 - 5568, 1980.

Randel, W. J., "Global atmospheric circulation statistics," NCAR Technical Note, NCAR/TN-295+STR, National Center for Atmospheric Research, Boulder, Co., 245 December 1987.

Raper, O. F., C. B. Farmer, R. Zander and J. H. Park, "Infrared spectroscopic measurements of halogenated sink and reservoir gases in the stratosphere from the ATMOS Spacelab 3 mission," J. Geophys. Res., 92, 9851 - 9858, 1987. 9858, 1987.

Rinsland, C. P., A. Goldman, V. Malathy Devi, B. Fridovich, D. G. Snyder, G. D. Jones, F. J. Murcray, D. G. Murcray, M. A. H. Smith, R. K. Seals. Jr., M. T. Coffey and W. G. Mankin, "Simultaneous stratospheric measurements of H_2O, HDO, and CH_4 from balloon-borne and aircraft infrared solar absorption spectra and tunable diode laboratory spectra of HDO," J. Geophys. Res., 89, 7259 - 7266, 1984.

Rinsland, C. P., A. Goldman, F. J. Murcray, D. G. Murcray, M. A. H. Smith, R. K. Seals, Jr., J. C. Larsen and P. L. Rinsland, "Stratospheric N_2O mixing ratio profile from high-resolution balloon-borne solar absorption spectra and laboratory spectra near 1880 cm^{-1}," Appl. Opt., 21, 4351 - 4355, 1982.

Rinsland, C. P., J. M. Russell III, J. H. Park and J. Namkung, "Retrieval of upper atmosphere pressure-temperature profiles from high resolution solar occultation spectra," NASA Technical Memorandum 89160, 1987.

Rinsland, C. P., R. Zander, L. R. Brown, C. B. Farmer, J. H. Park, R. H. Norton, J. M. Russell III and O. F. Raper, "Detection of carbonyl fluoride in the stratosphere," Geophys. Res. Letts., 13, 769-772, 1986a.

Rinsland, C. P., R. Zander, C. B. Farmer, R. H. Norton, L. R. Brown, J. M. Russell III and J. H. Park, "Evidence for the presence of the 802.7 cm^{-1} band Q branch of HO_2NO_2 in high-resolution solar absorption spectra of the stratosphere," Geophys. Res. Letts., 13, 761-764, 1986b.

Rinsland, C. P., R. Zander, J. S. Namkung, C. B. Farmer and R. H. Norton, "Stratospheric infrared continuum absorptions observed by the ATMOS instrument," submitted 1989.

Remsberg, E. E., J. M. Russell III, L. L. Gordley, J. C. Gille and P. L. Bailey, "Implications of the stratospheric water vapor distribution as determined from the Nimbus 7 LIMS experiment," J. Atmos. Sci., 41, 2934 - 2945, 1984.

Rothman, L. S., R. R. Gamache, A. Barbe, A. Goldman, J. R. Gillis, L. R. Brown, R. A. Toth, J.-M. Flaud and C. Camy-Peyret, "AFGL atmospheric absorption parameters compilation: 1982 edition," Appl. Opt., 22, 2247 - 2256, 1983.

Rothman, L. S., R. R. Gamache, A. Goldman, L. R. Brown, R. A. Toth, H. M. Pickett, R. L. Poynter, J.-M. Flaud, C. Camy-Peyret, A. Barbe, N. Husson, C. P. Rinsland, and M. A. H. Smith, "The HITRAN database: 1986 edition," Appl. Opt., 26, 4058 - 4096, 1987.

Russell III, J. M., C. B. Farmer, C. P. Rinsland, R. Zander, L. Froidevaux, G. C. Toon, B. Gao, J. Shaw and M. R. Gunson, "Measurements of odd nitrogen compounds in the stratosphere by the ATMOS experiment on Spacelab 3," J. Geophys. Res., 93, 1718 - 1736, 1988.

Schmidt, U., G. Kulessa, E. Klein, E.-P. Roth, P. Fabian, and R. Borchers, "Intercomparison of balloon-borne cryogenic whole air samplers during the MAP/GLOBUS 1983 campaign," Planet. Space Sci., 35, 647 - 656, 1987.

Solomon, S. and R. R. Garcia, "On the distribution of long-lived tracers and chlorine species in the middle atmosphere," J. Geophys. Res., 89, 11633 - 11644, 1984.

Solomon, S., R. R. Garcia, J. J. Olivero, R. M. Bevilacqua, P. R. Schwartz, R. T. Clancy and D. O. Muhleman, "Photochemistry and transport of carbon monoxide in the middle atmosphere," J. Atmos. Sci., 42, 1072, (1985).

Toon, G. C., C. B. Farmer and R. H. Norton, "Detection of stratospheric N_2O_5 by infrared remote sounding," Nature, 319, 570 - 571, 1986.

Vercheval, J., C. Lippens, C. Muller, M. Ackerman, M. P. Lemaitre, J. Besson, A. Girard and J. Laurent, "CO_2 and CO vertical distribution in the middle atmosphere and lower thermosphere deduced from infrared spectra," Ann. Geophys. 4A, 161 - 164, (1986).

World Meteorological Organization, "Atmospheric ozone 1985: Assessment of our understanding of the processes controlling the present distribution and change," Report No. 16, WMO Global Ozone Research Monitoring Project, Geneva, Switzerland, 1986.

Zander, R., C. P. Rinsland, C. B. Farmer, L. R. Brown and R. H. Norton, "Observation of several chlorine nitrate ($ClONO_2$) bands in stratospheric infrared spectra," Geophys. Res. Letts., 13, 757-760, 1986.

Zander, R., C. P. Rinsland, C. B. Farmer and R. H. Norton, "Infrared spectroscopic measurements of halogenated source gases in the stratosphere with the ATMOS instrument," J. Geophys. Res., 92, 9836 - 9850, 1987.

Table 1.

ATMOS/Spacelab 3 Occultations Analyzed in this Study

Occultation synonym	Filter number*	Date day/month of 1985	GMT** hr:min:sec	Latitude**	Longitude**
Sunsets					
SS02	1	30/4	10:54:22	32.8°N	115.5°W
SS03	2	30/4	13:57:38	32.2	69.5
SS05	1	30/4	18:32:33	31.4	0.4
SS06	3	30/4	23:07:26	30.5	291.5
SS07	2	1/5	00:39:06	30.2	268.4
SS08	1	1/5	02:10:43	29.9	245.4
SS09	3	1/5	17:27:07	26.8	15.3
SS11	3	1/5	20:30:25	26.3	329.3
SS12	2	1/5	22:02:03	26.0	306.3
SS13	3	1/5	23:33:40	25.6	283.2
Sunrises					
SR02	3	30/4	11:29:58	48.8°S	294.3°W
SR05	2	1/5	08:52:40	47.0	332.8
SR06	1	1/5	10:24:17	46.9	309.9

* filter #1 covered 600 - 1190 cm^{-1}
  filter #2 1100 - 2000 cm^{-1}
  filter #3 1580 - 3400 cm^{-1}
Filter 1 and 2 data were recorded with a 2 mrad field-of-view (FOV) corresponding to a 4 km vertical FOV at the horizon. Filter 3 data were recorded with a 1 mrad FOV, corresponding to a 2 km vertical FOV at the horizon.

**time and location of the spectra in the occulations closest to a tangent height of 30 km

Table 2

Spectral Regions Used To Retrieve The Profiles Reported In This Study

Molecule	z (km)	Wavenumber region (cm^{-1})	Band	Line strength (cm.molecule-1)
CO	10-110	2065-2190	1-0	$4x10^{-19}$-10^{-20}
CH_4	30-65	1240-1380	ν_4	10^{-19}-10^{-20}
	10-35	1420-1600	ν_2	10^{-21}-10^{-23}
	10-35	2650-2710	$2\nu_4$	10^{-21}-10^{-23}
	10-50	2820-2880	$\nu_2+\nu_4$	10^{-20}-10^{-21}
	25-65	2940-3070	ν_3	0^{-19}-10^{-21}
N_2O	20-45	1185-1195	$2\nu_2$	$3-6x10^{-21}$
	25-55	1255-1305	ν_1	$2x10^{-19}$-10^{-20}
	10-30	1880 ± 1 (Q-branch)	$\nu_1+\nu_2$	10^{-22}-10^{-23}
	30-55	2195-2215	ν_3	10^{-18}-10^{-19}
	20-45	2440-2460	$\nu_1+2\nu$	$3-5x10^{-21}$
	25-50	2550-2585	$2\nu_1$	$-2x10^{-20}$
O_3	10-100	1050-1080	ν_3	$5x10^{-20}$-10^{-22}
	10-55	1100-1180	ν_1	10^{-21}-10^{-22}
H_2O		1360-1980	ν_2*	
	60-90			$>10^{-19}$
	50-80			10^{-19}-10^{-20}
	35-70			10^{-20}-10^{-21}
	25-60			10^{-21}-10^{-22}
	10-50			10^{-22}-10^{-24}

* for H_2O these are listed by order of magnitude of line strength of transitions in the ν_2

Table 3

Error Budget for Species Included In This Study

Relative 1σ Error (%) in VMR For An Individual Occultation

Error Source	Error Type	CH_4		N_2O		CO	H_2O		O_3*	
		F2	F3	F2	F3	F3	F2	F3	F1	F2
I. Observational Geometry										
a) Reference pressure	S	2	2	2	2	2	2	2	2	2
b) Tangent pressure	R	3-8	5-8	3-8	5-8	5-8	3-8	5-8	8	5-8
c) Temperature profile	R	1	1	1	1	1	1	1	1	1
II. Algorithm	S	<5	<5	<5	<5	<5	<5	<5	<5	<5
III. Observational Data										
a) Finite SNR	R	2	3	2	3	3	2	3	2	2
b) Zero Transmission	R	2	5	2	5	5	2	5	2	2
Offsets	S	1	2	1	2	2	1	2	1	1
IV. Spectroscopic Parameters	S	5	5	5	5	3	5	5	10	10
Total Systematic Error		7	8	7	8	8	7	8	11	11
Total Random Error		4-9	8-10	4-9	8-10	8-10	4-9	8-10	9	4-9

Table 4a

Volume mixing ratio-height profiles derived in this study

Sunset

HEIGHT (KM)	PRESS. (mb)	TEMP. (K)	CH_4 (ppmv)	N_2O (ppmv)	H_2O (ppmv)	O_3 (ppmv)	CO (ppmv)
14.0	149.45	203.6	1.62(32)	0.31(5)	7.0(18)	0.27(4)	3.6 (8)E-2
18.0	77.21	207.6	1.51(19)	0.27(3)	3.4(5)	1.3 (3)	2.1 (6)E-2
22.0	40.58	214.6	1.24(17)	0.19(3)	4.7(5)	3.7 (6)	9.9 (12)E-3
26.0	21.84	223.1	0.94(16)	0.10(3)	4.9(7)	6.5 (10)	1.1 (1)E-2
30.0	12.06	232.1	0.75(12)	5.0(17)E-2	5.5(6)	7.9 (11)	1.5 (2)E-2
34.0	6.79	239.4	0.77(12)	4.5(7)E-2	5.5(6)	8.0 (12)	2.0 (3)E-2
38.0	3.92	251.2	0.82(12)	4.5(9)E-2	5.5(7)	6.7 (10)	2.6 (4)E-2
42.0	2.32	261.8	0.69(12)	3.4(8)E-2	5.8(8)	4.7 (8)	3.2 (4)E-2
46.0	1.39	271.6	0.53(13)	2.0(6)E-2	6.2(7)	3.6 (6)	3.9 (9)E-2
50.0	0.85	272.1	0.41(9)	1.0(3)E-2	6.6(9)	2.8 (5)	4.0 (10)E-2
54.0	0.52	264.1	0.32(7)	4.0(12)E-3	6.6(9)	2.0 (4)	5.4 (13)E-2
58.0	0.31	252.9	0.22(4)	1.6(6)E-3	6.6(9)	1.2 (2)	7.8 (19)E-2
62.0	0.18	241.3	0.14(2)	5.8(24)E-4	6.1(11)	0.78(12)	0.11(4)
66.0	0.10	228.7	0.10(2)		5.5(8)	0.50(10)	0.23(8)
70.0	5.57E-2	218.6			4.5(5)	0.24(4)	0.43(13)
74.0	2.98E-2	209.6			3.7(6)	9.2 (14)E-2	1.1 (4)
78.0	1.56E-2	202.0			2.7(4)	9.7 (19)E-2	2.7 (10)
82.0	7.97E-3	194.6			1.6(4)	0.26(8)	6.0 (16)
86.0	3.98E-3	187.9			0.7(3)	0.61(11)	10 (2)
90.0	1.96E-3	188.0				0.91(15)	15 (3)
94.0	9.70E-4	189.6				0.59(13)	20 (4)
98.0	4.90E-4	197.8					30 (5)
102.0	2.59E-4	216.9					38 (7)
106.0	1.47E-4	241.7					43 (10)

Read E-2 as 10^{-2}. All uncertainties in parentheses are in units of the least significant figure.

Table 4b

Volume mixing ratio-height profiles derived in this study.

Sunrise

HEIGHT (KM)	PRESS. (mb)	TEMP. (K)	CH_4 (ppmv)	N_2O (ppmv)	H_2O (ppmv)	O_3 (ppmv)	CO (ppmv)
14.0	144.89	212.8	1.60(35)	0.29(3)	3.7(7)	0.72(11)	1.0 (2)E-2
18.0	76.25	210.8	1.35(17)	0.22(4)	4.9(9)	1.8 (3)	1.2 (1)E-2
22.0	40.33	215.5	1.11(18)	0.18(2)	4.5(9)	3.6 (5)	1.3 (2)E-2
26.0	21.53	216.8	1.01(23)	0.13(2)	4.9(11)	5.2 (8)	1.5 (3)E-2
30.0	11.55	219.0	0.87(14)	7.9 (12)E-2	5.3(11)	5.7 (10)	1.4 (2)E-2
34.0	6.26	223.2	0.77(17)	5.0 (8)E-2	5.7(22)	6.6 (12)	1.3 (4)E-2
38.0	3.43	228.4	0.58(11)	2.2 (8)E-2	5.9(20)	7.2 (16)	1.4 (8)E-2
42.0	1.92	234.8	0.41(8)	7.5 (37)E-3	6.5(18)	6.6 (12)	2.2 (19)E-2
46.0	1.09	240.9	0.30(8)	4.1 (24)E-3	7.2(24)	4.7 (10)	5.4 (48)E-2
50.0	0.63	242.3	0.25(3)	2.0 (11)E-3	7.0(20)	2.5 (8)	0.15(12)
54.0	0.36	238.0	0.20(3)	1.3 (9)E-3	6.4(19)	1.5 (10)	0.38(28)
58.0	0.20	236.5	0.16(8)		6.3(25)	1.1 (6)	1.1 (8)
62.0	0.12	234.0	0.10(3)		5.9(26)	0.31(19)	2.4 (8)
66.0	6.43E-2	226.4			4.6(19)	6.6 (40)E-2	3.7 (16)
70.0	3.51E-2	213.2			5.0(21)	6.40E-3*	5.4 (19)
74.0	1.85E-2	205.2			4.3(12)	1.90E-3*	8.3 (26)
78.0	9.54E-3	197.5			3.5(12)	5.20E-4*	14 (6)
82.0	4.80E-3	190.5			2.2(7)	7.3 (44)E-2	23 (8)
86.0	2.37E-3	188.1			0.8(5)	0.84(24)	33 (10)
90.0	1.18E-3	189.4				1.5 (4)	42 (12)
94.0	5.87E-4	194.1				1.3 (5)	47 (12)
98.0	3.04E-4	209.4					45 (12)
102.0	1.68E-4	232.8					

Read E-2 as 10^{-2}. All uncertainties in parentheses are in units of the least significant figure.

* These represent upper limit values only for O_3 at sunrise.

List of figures and captions.

Figure 1 - Trace (a) the 'pure' solar spectrum created by averaging spectra from the beginning of the SS07 occultation event. Trace (b) a 'raw' unratioed spectrum characterized by the uneven filter transmission, increasing solar CO absorptions at higher frequencies, and the many sharp telluric absorption features. Trace (c) the derived ratio spectrum showing a consistent 100% transmission level and residual absorption features of telluric H_2O, CH_4, and CO_2. The original interferogram was recorded at 00:38:53 G.M.T. on May 1, 1985, at a nominal tangent height of 54 km over latitude 30.6°N, longitude 268.6°W.

Figure 2 - A smaller portion of the spectra plotted in Fig. 1. The solar spectrum (a) and the unratioed spectrum (b) have been scaled and offset from the telluric absorption spectrum (c). The pairs of lines in the central spectrum are assigned as telluric and instrumental H_2O absorption features, Doppler shifted from each other by the relative motion of the spacecraft to the earth.

Figure 3 - Three components of the $J = 7 \leftarrow 6$ transition in the $^{12}CH_4$ ν_4 fundamental have been used in the NLLD inverse method. The lower trace is the difference between the upper observed and a calculated spectra.

Figure 4 - Comparison of results of CH_4 profiles inferred from the SS07 occultation using four independent inversion methods as described in the text. The 1σ error bars plotted for one profile are typical of the precision achieved by these retrieval schemes.

Figure 5 - Methane profiles inferred from the seven filter #2 and #3 sunset occultations using the NLLD algorithm.

Figure 6 - The mean zonal CH_4 profiles representative of the sunset (28°N) and sunrise (48°S) occultation results, with 1σ error bars representative of the accuracy at occassional heights.

Figure 7 - Nitrous oxide profiles from the seven filter #2 and #3 sunset occultations inferred using the NLLD algorithm.

Figure 8 - The mean zonal profiles for N_2O at sunset (28°N) and sunrise (48°S), with 1σ total error bars at occasional heights as for the CH_4 profiles in Fig. 6.

Figure 9 - The CO mixing ratio values inferred from the four sunset filter #3 occultations used in forming the 28°N mean zonal profile plotted in Figure 10.

Figure 10 - The mean zonal CO vmr profile for 28°N and the profile inferred from the single sunrise occultation, SR02.

Figure 11 - The H_2O vmr values inferred from the seven filter #2 and #3 sunset occultation spectra.

Figure 12 - The H_2O profiles inferred from SR02 and SR05 occultations. The mean of these profiles, with an uncertainty found as the RSS of random errors added to the total systematic error (8%), is given in Table 4.

Figure 13 - Water vapor profiles measured by several experiments at low northern mid-latitudes. The values labelled 'MICROWAVE' are

estimates of the average water vapor at those altitudes (with a range of ±0.5 ppmv) measured by a ground-based microwave spectrometer located at JPL (34°N) between late April and early May 1985 (Bevilacqua et al. 1987).

Figure 14 - The hydrogen budget as defined by combining the H_2O and CH_4 mean zonal vmr profiles for 28°N (see equation (1)). Error bars were computed as an appropriately weighted RSS of the random errors associated with the H_2O and CH_4 profiles added to the estimated total systematic error (9%).

Figure 15 - The O_3 vmr values inferred from the six filter #1 and #2 sunset occultations.

Figure 16 - The O_3 vmr values from the sunrise SR05 and SR06 occultations.

Figure 17 - The mean zonal O_3 vmr-height profiles reported in this present work and the range of O_3 vmr values measured by SAGE II McCormick, unpublished research) from April 26 to April 30 1985, over a 10° latitude band closest to the ATMOS SL-3 occultation events.
(a) Sunset measurements from both instruments around 28°N.
(b) Sunrise measurements from both instruments around 48°S.

Figure 18 - Stratospheric ozone profiles inferred from ATMOS Spacelab-3 spectra, using (A) the ν_1 fundamental band around 9.6 μm and based on the line parameters from Flaud et al. (1987), and (B) for the same lines based on the parameters of Pickett et al. (1985), (C) the combination bands $\nu_1+\nu_2$ and $\nu_2+\nu_3$ around 5.8 μm, (D) the combination band $\nu_1+\nu_3$ at 4.8 μm.

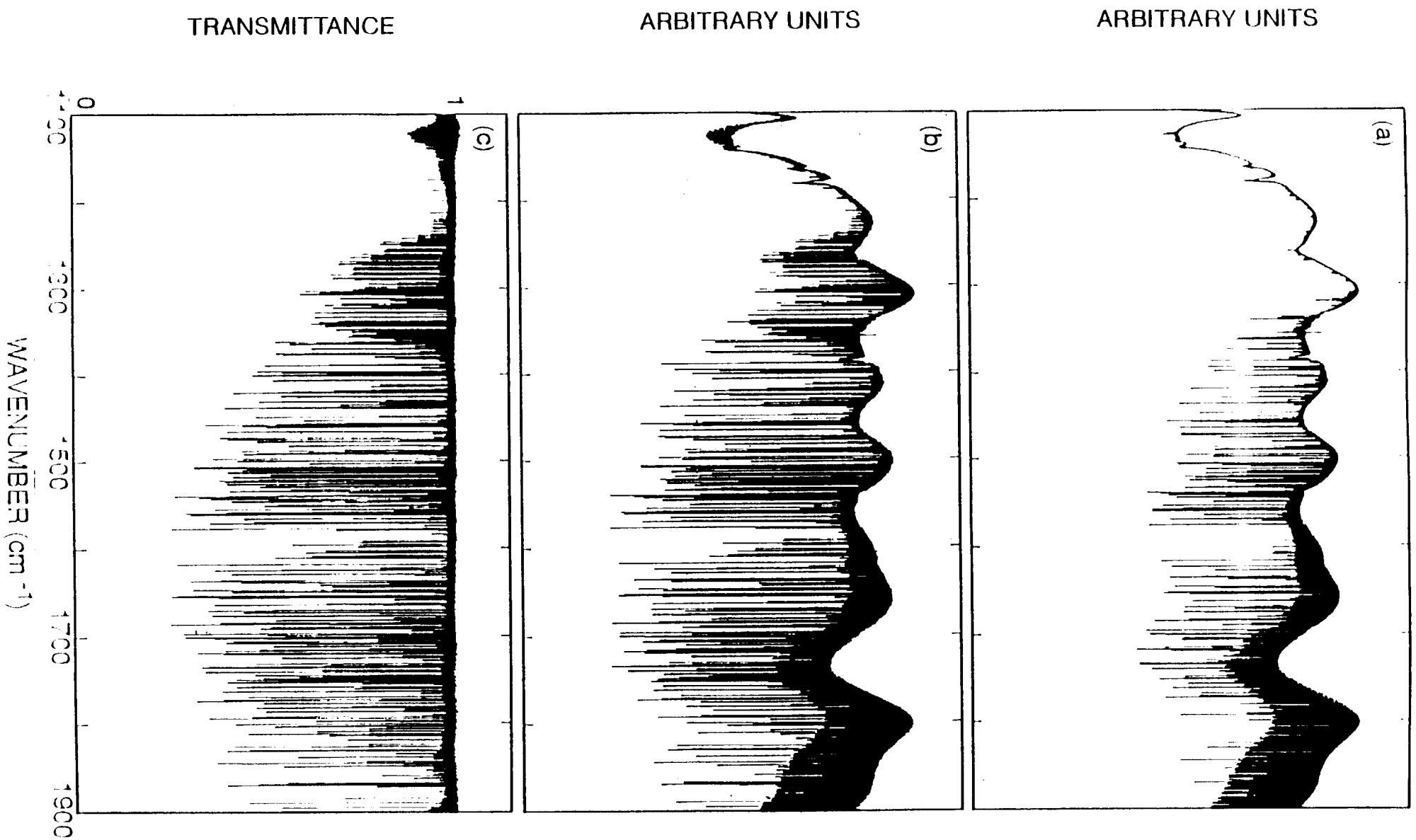

FIGURE 1

M.R. GUNSON ET AL.

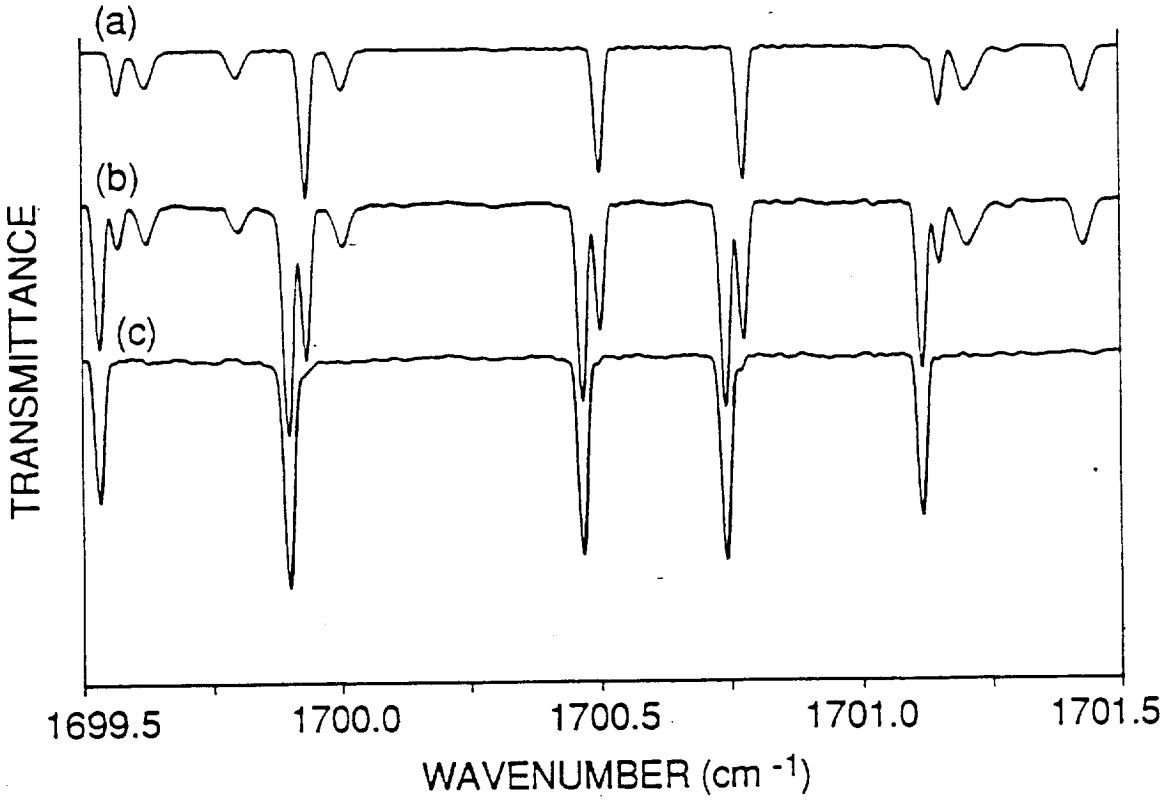

FIGURE 2

M.R. GUNSON ET AL.

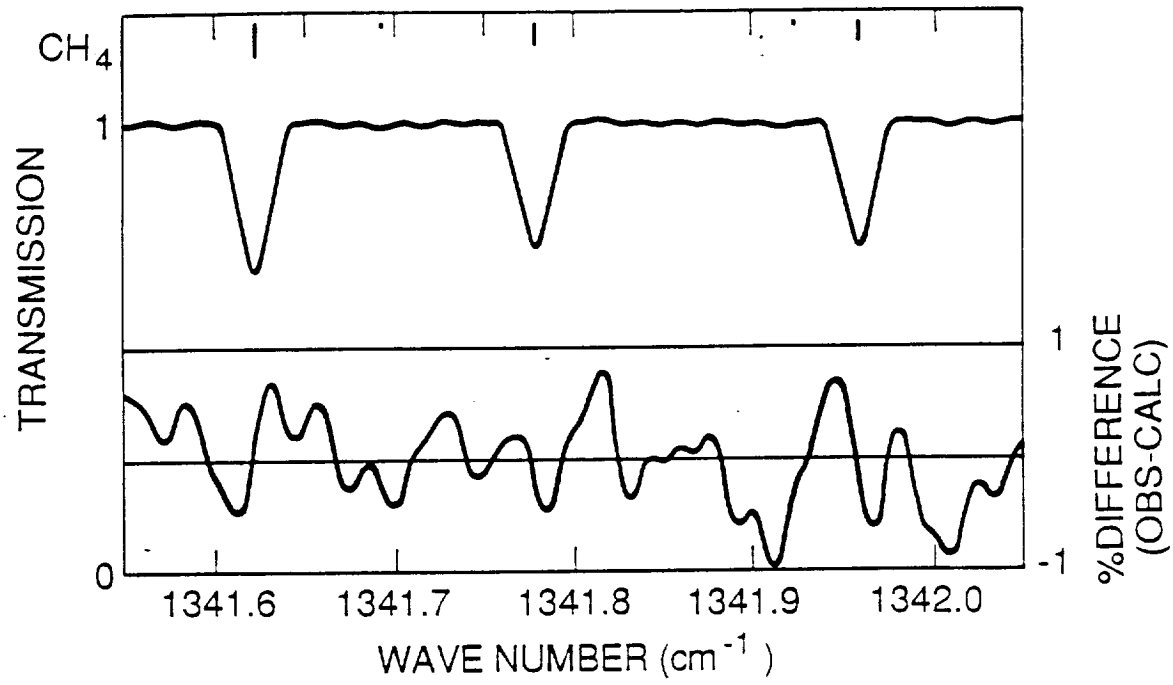

FIGURE 3

M.R. GUNSON ET AL.

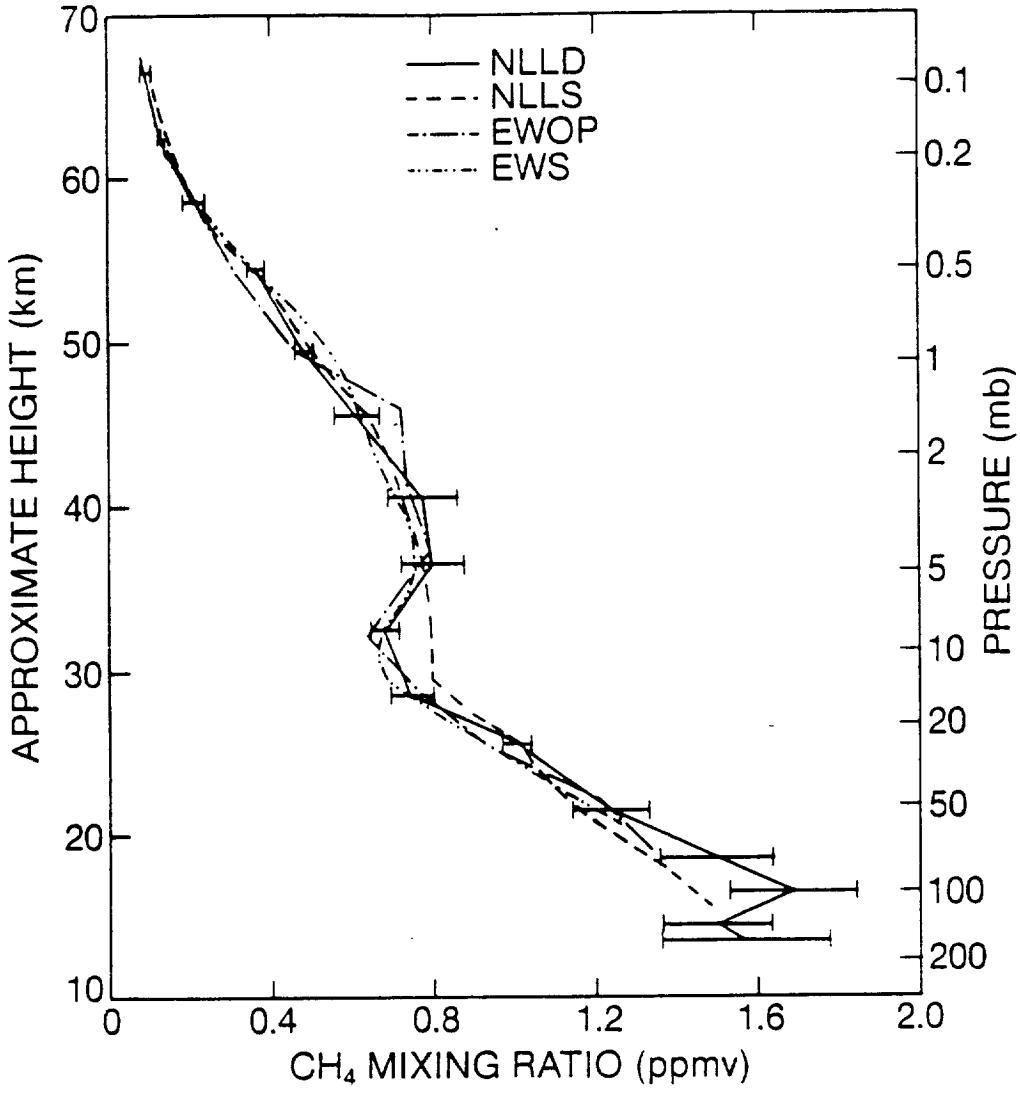

FIGURE 4

M.R. GUNSON ET AL.

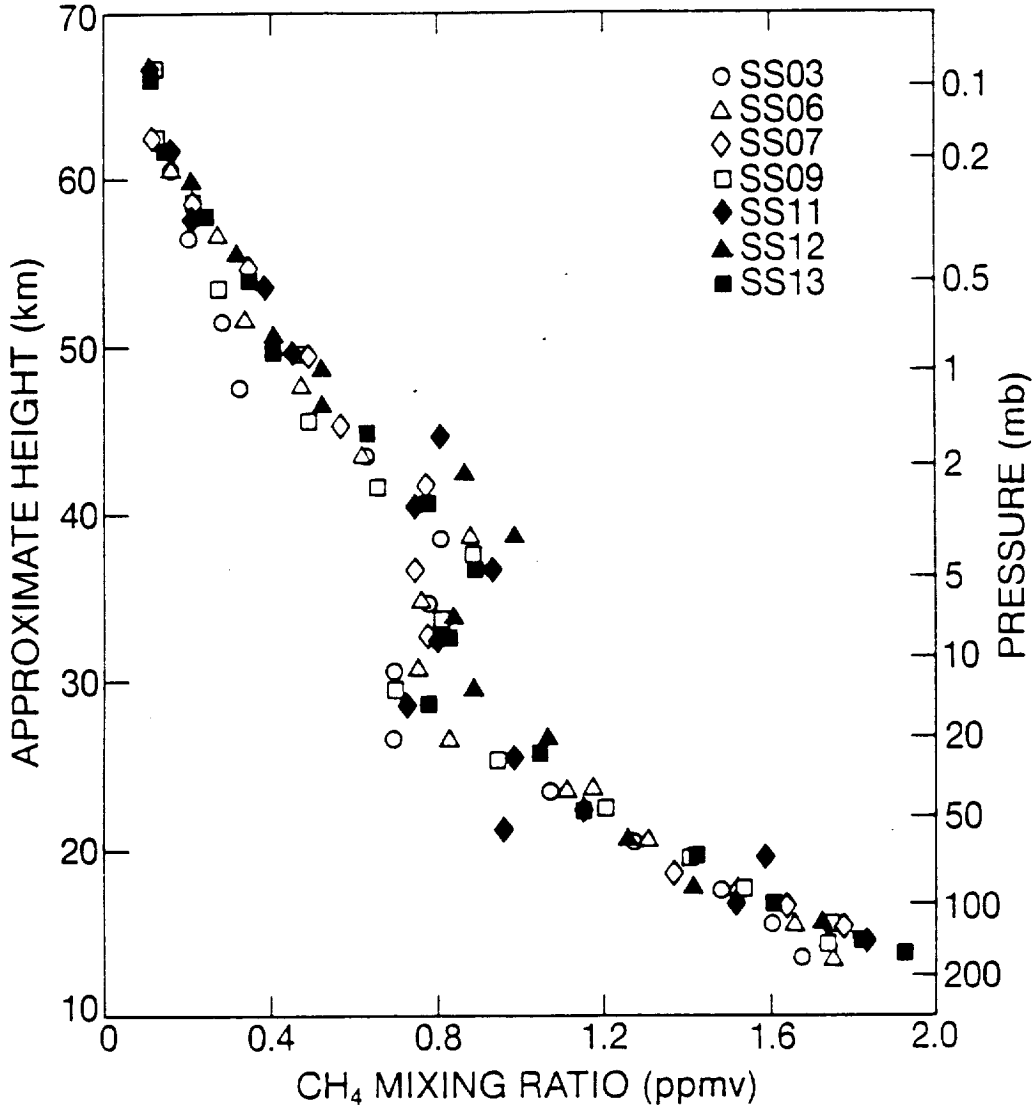

FIGURE 5

M.R. GUNSON ET AL.

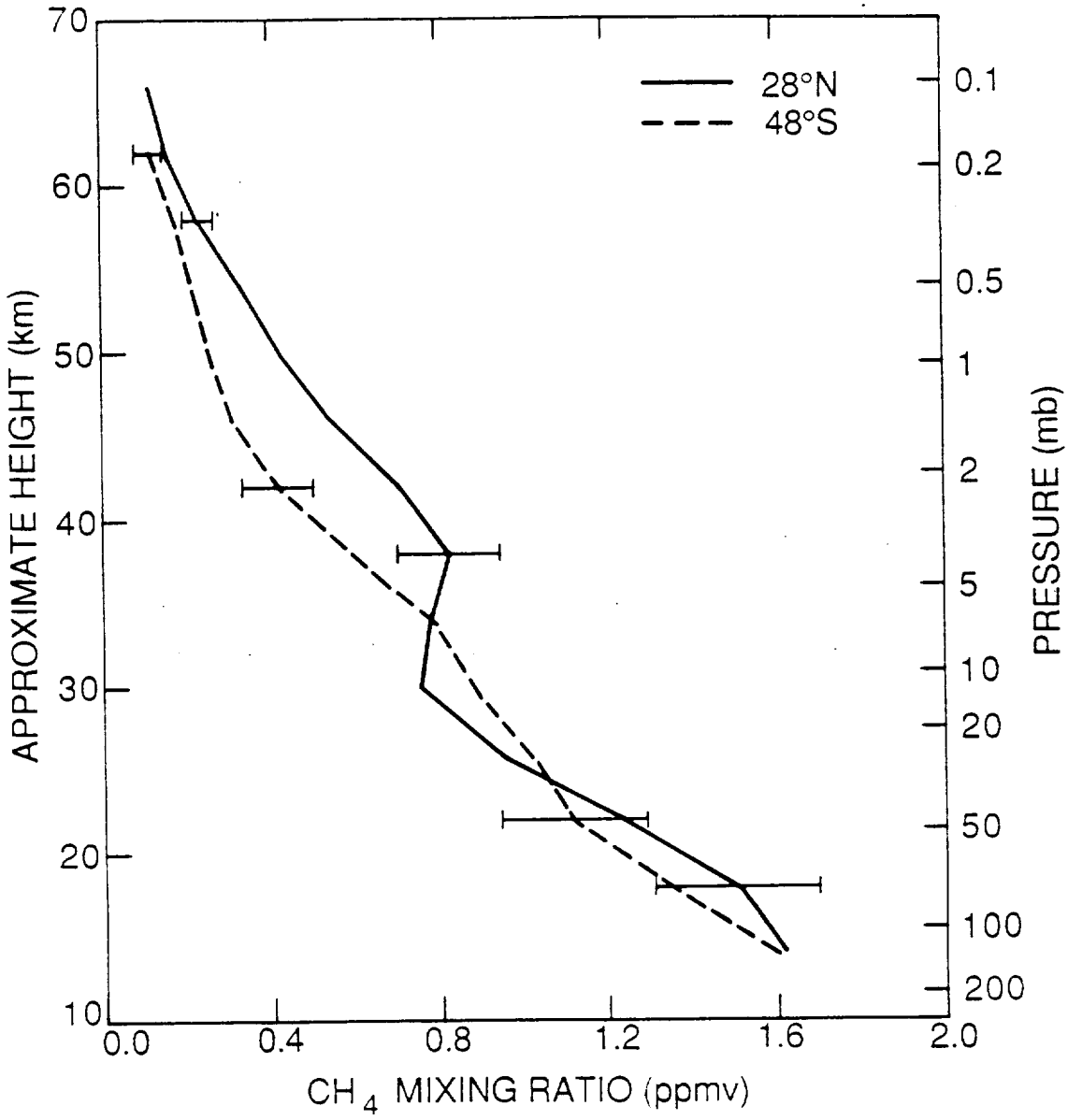

FIGURE 6

M.R. GUNSON ET AL.

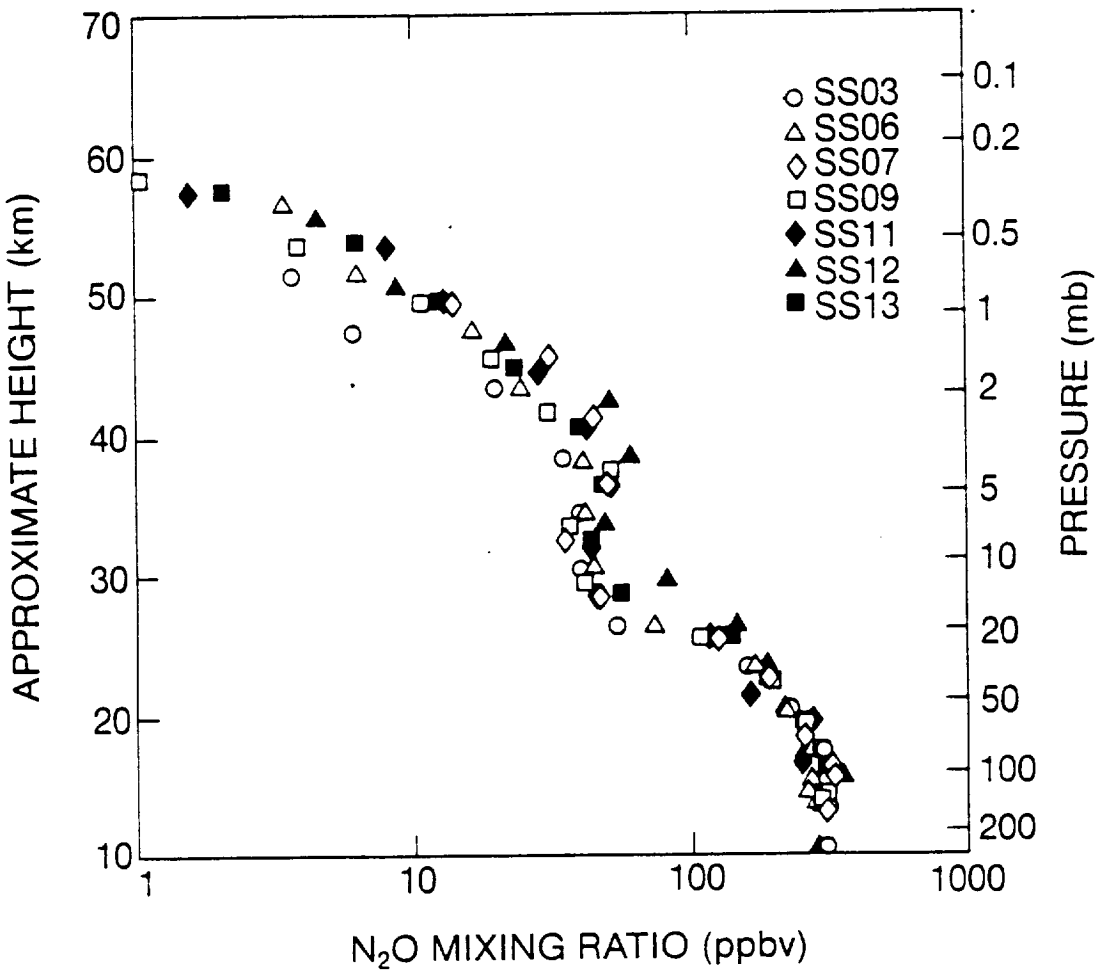

FIGURE 7

M.R. GUNSON ET AL.

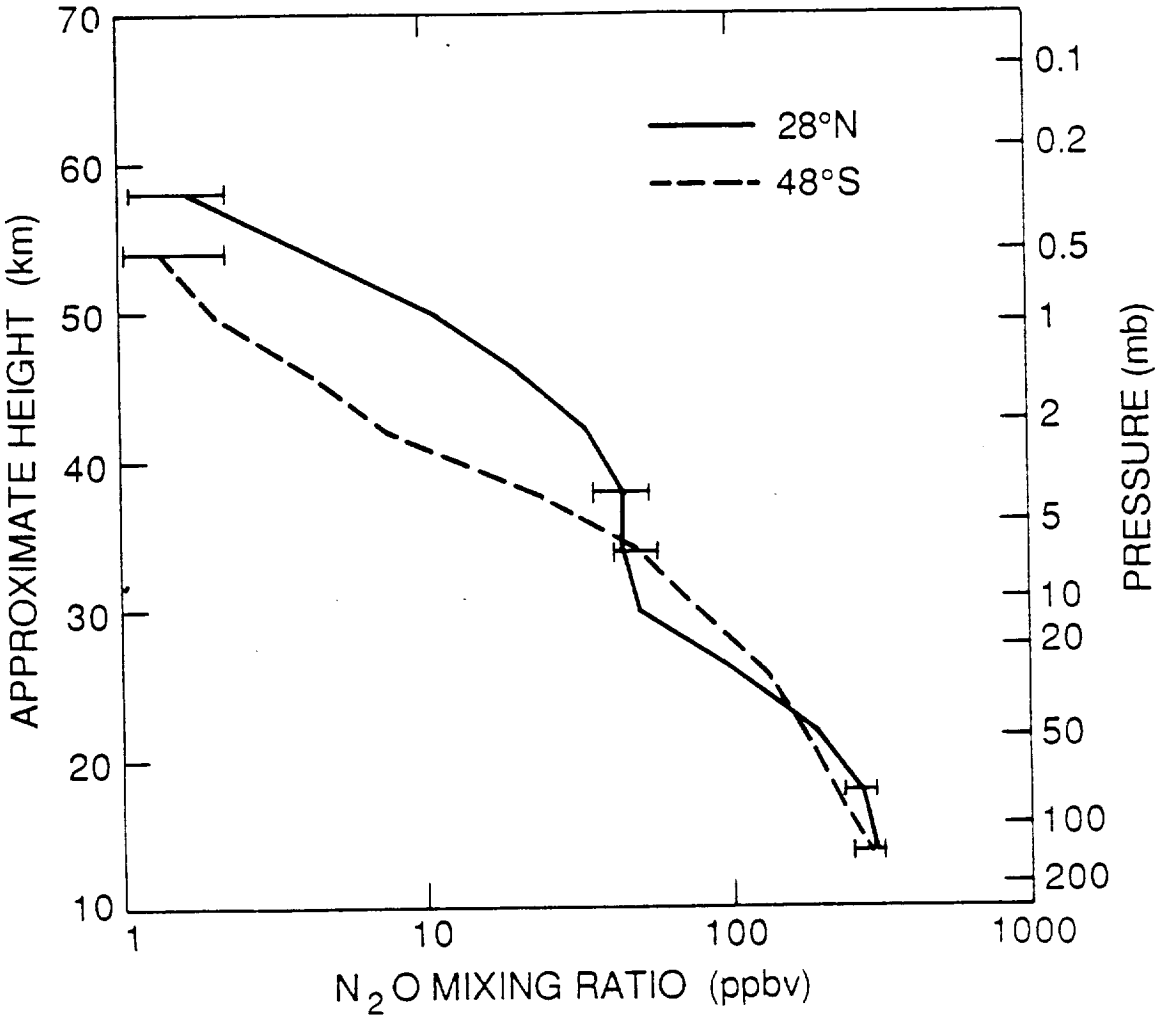

FIGURE 8

M.R. GUNSON ET AL.

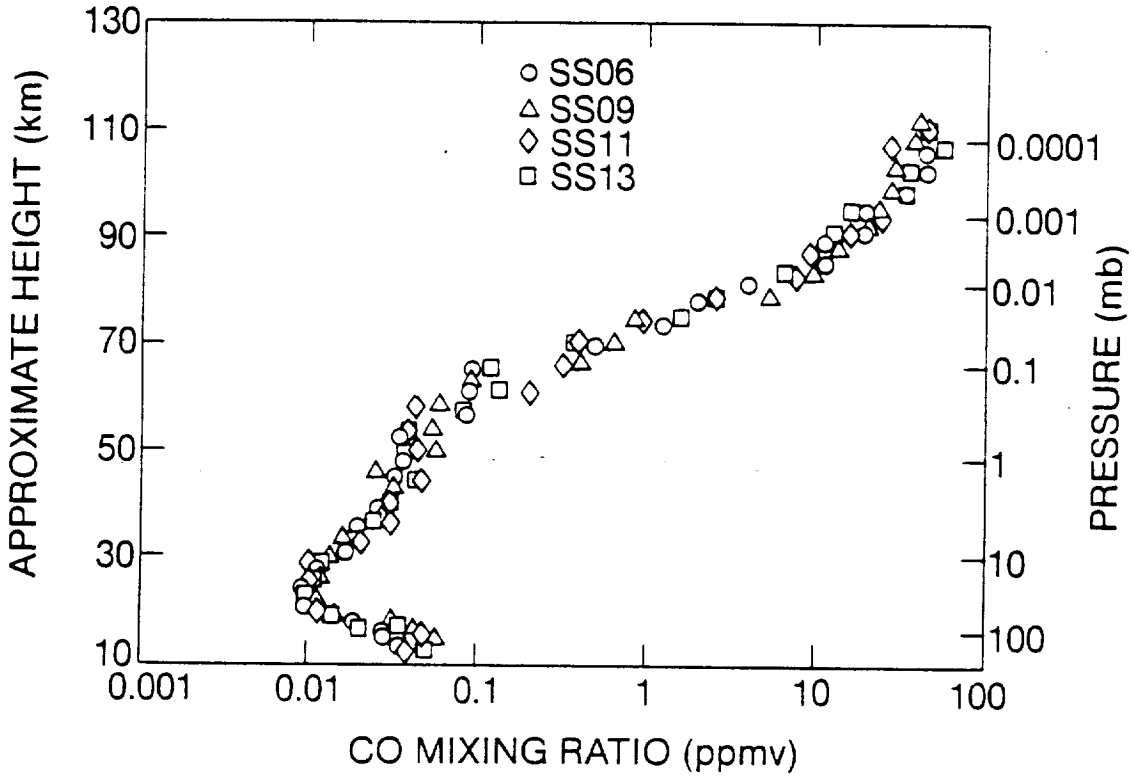

FIGURE 9

M.R. GUNSON ET AL.

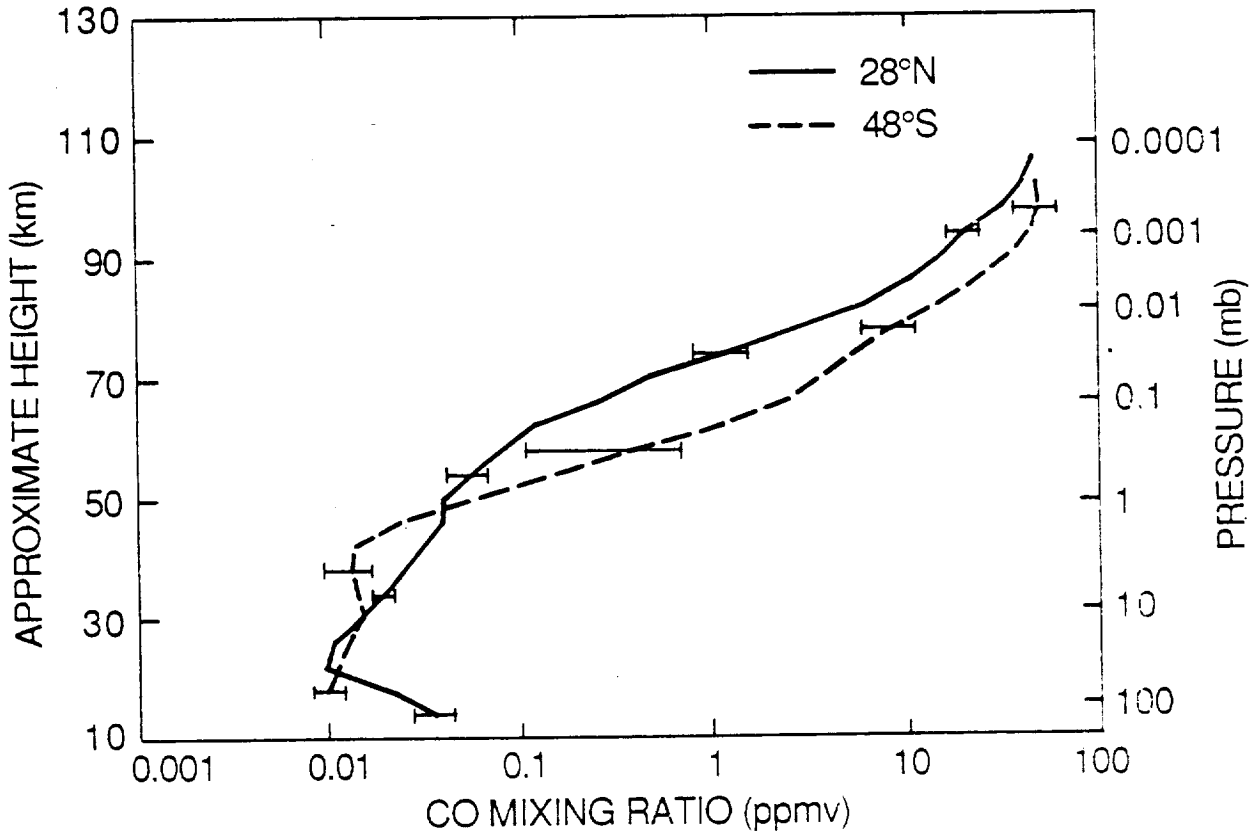

FIGURE 10
M.R. GUNSON ET AL.

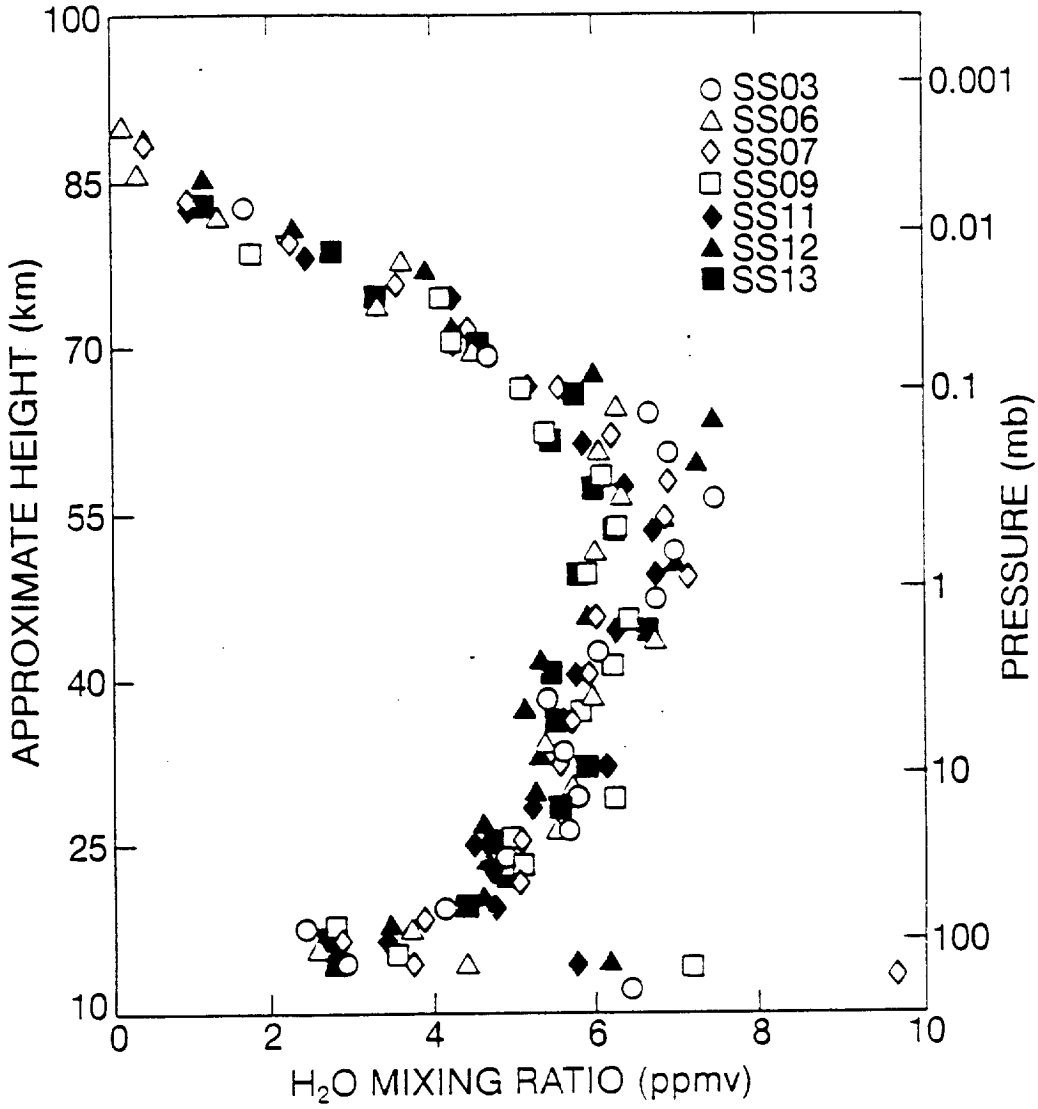

FIGURE 11

M.R. GUNSON ET AL.

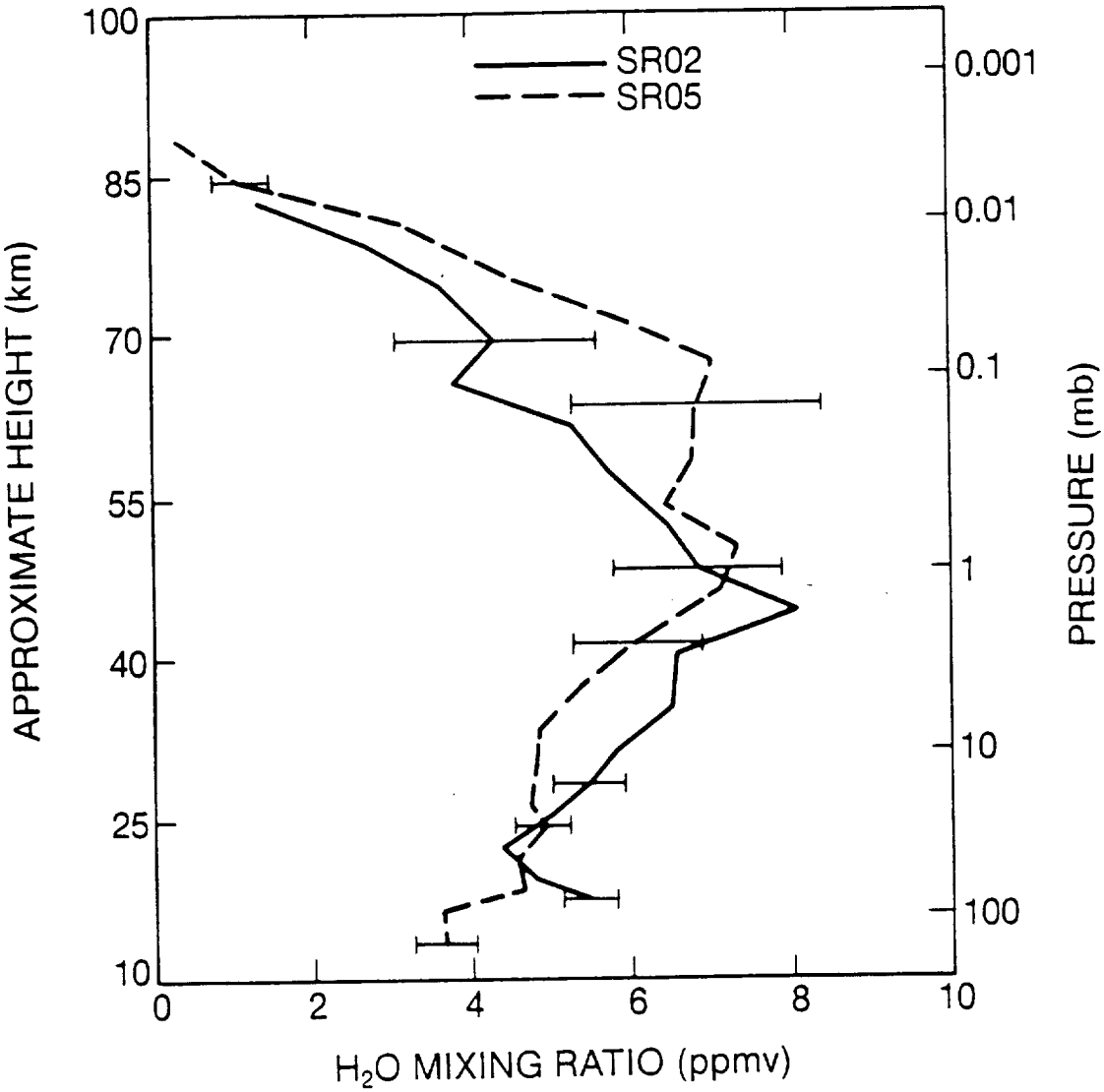

FIGURE 12

M.R. GUNSON ET AL.

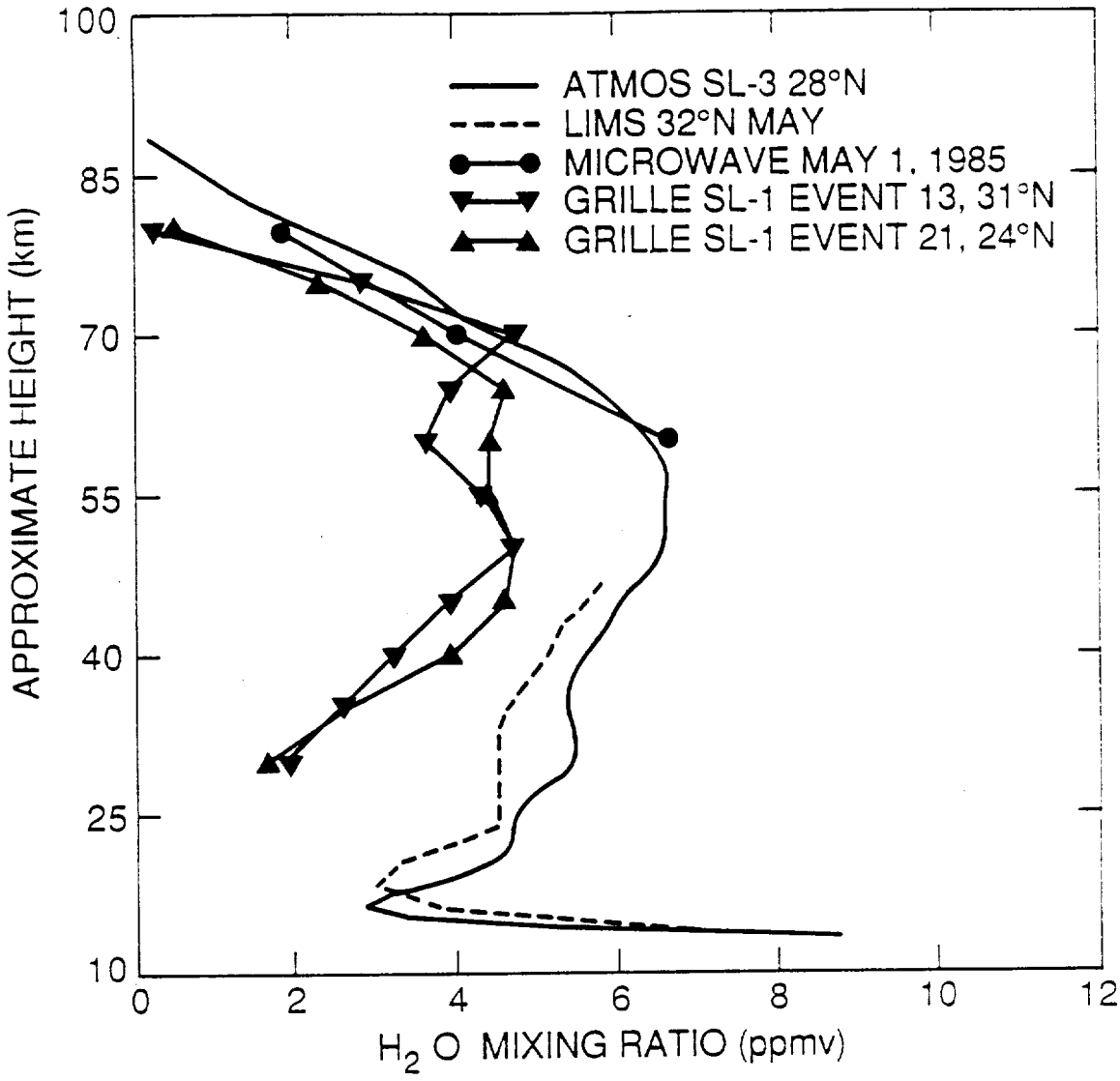

FIGURE 13

M.R. GUNSON ET AL.

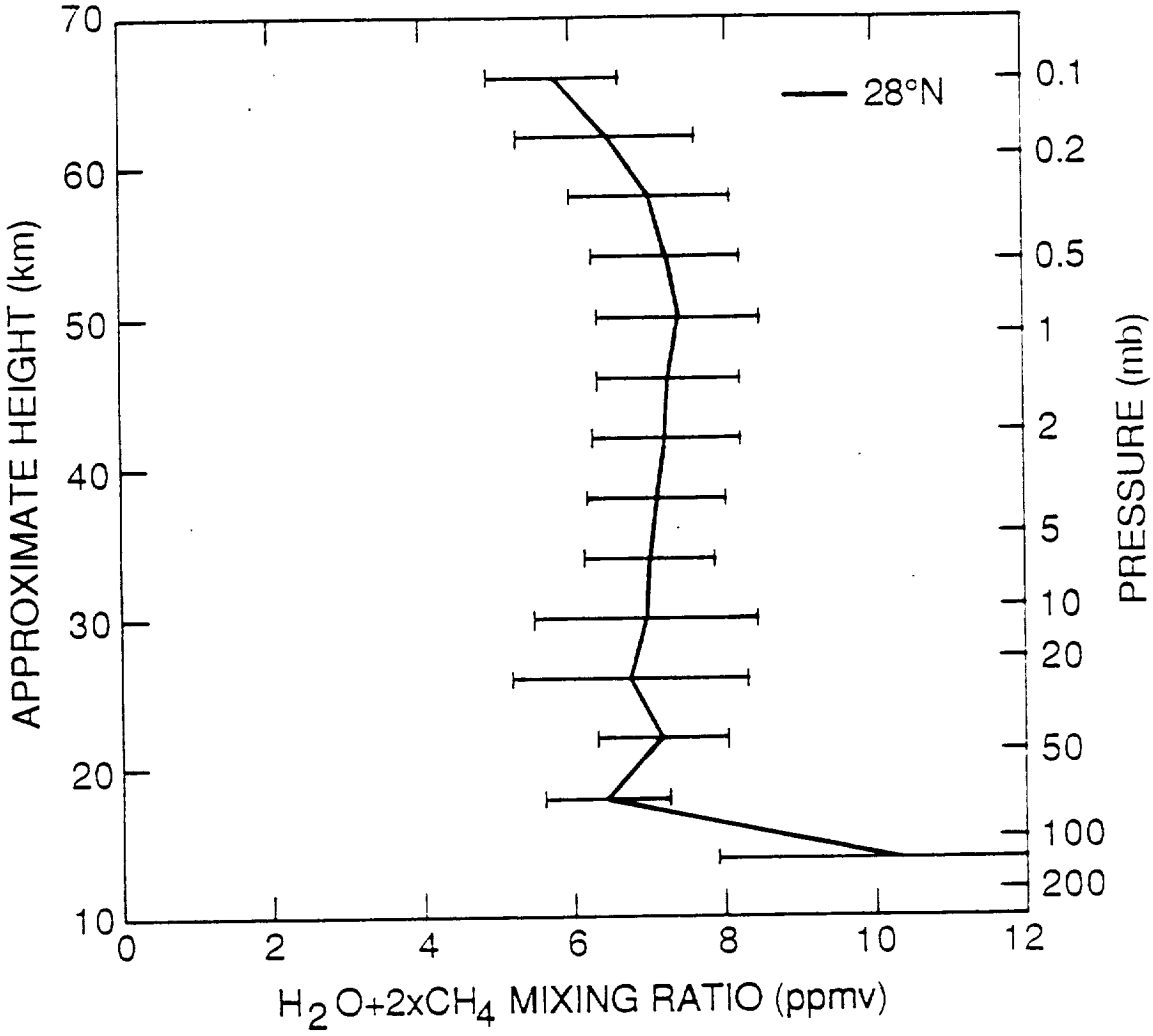

FIGURE 14

M.R. GUNSON ET AL.

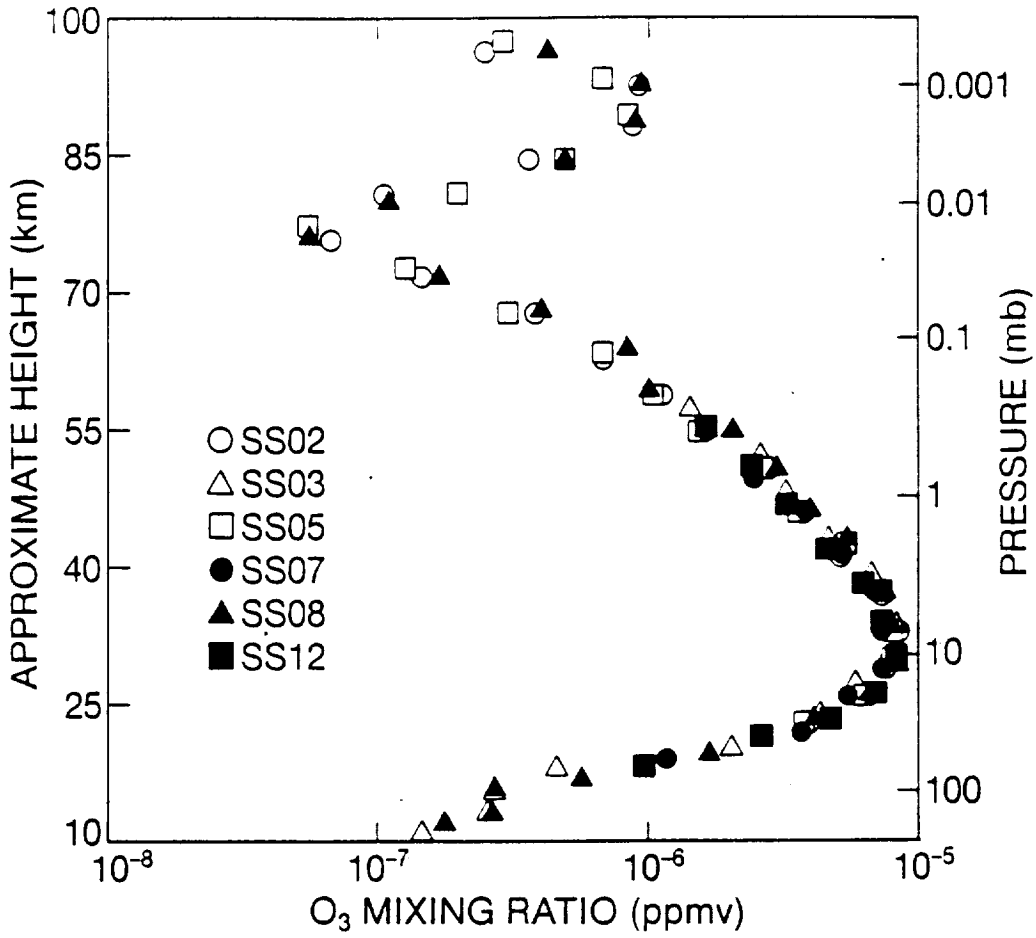

FIGURE 15

M.R. GUNSON ET AL.

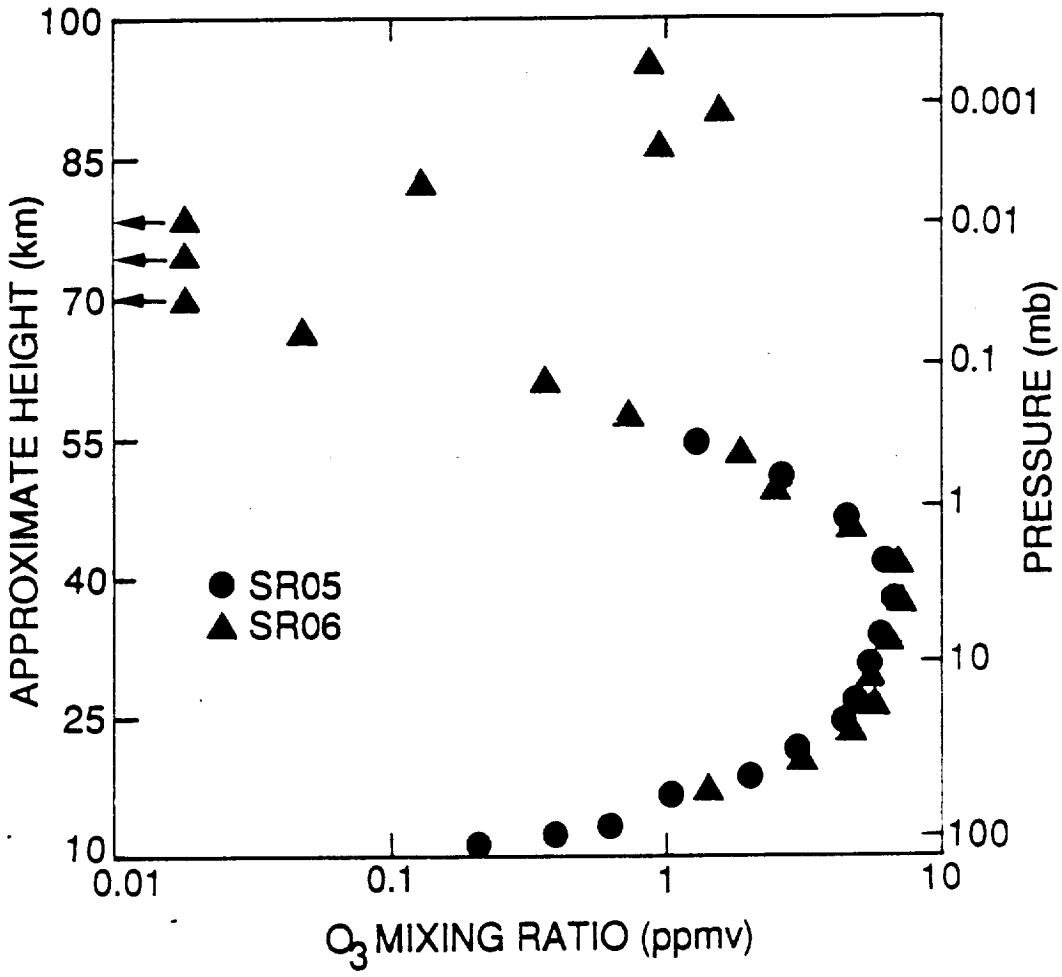

FIGURE 16

M.R. GUNSON ET AL.

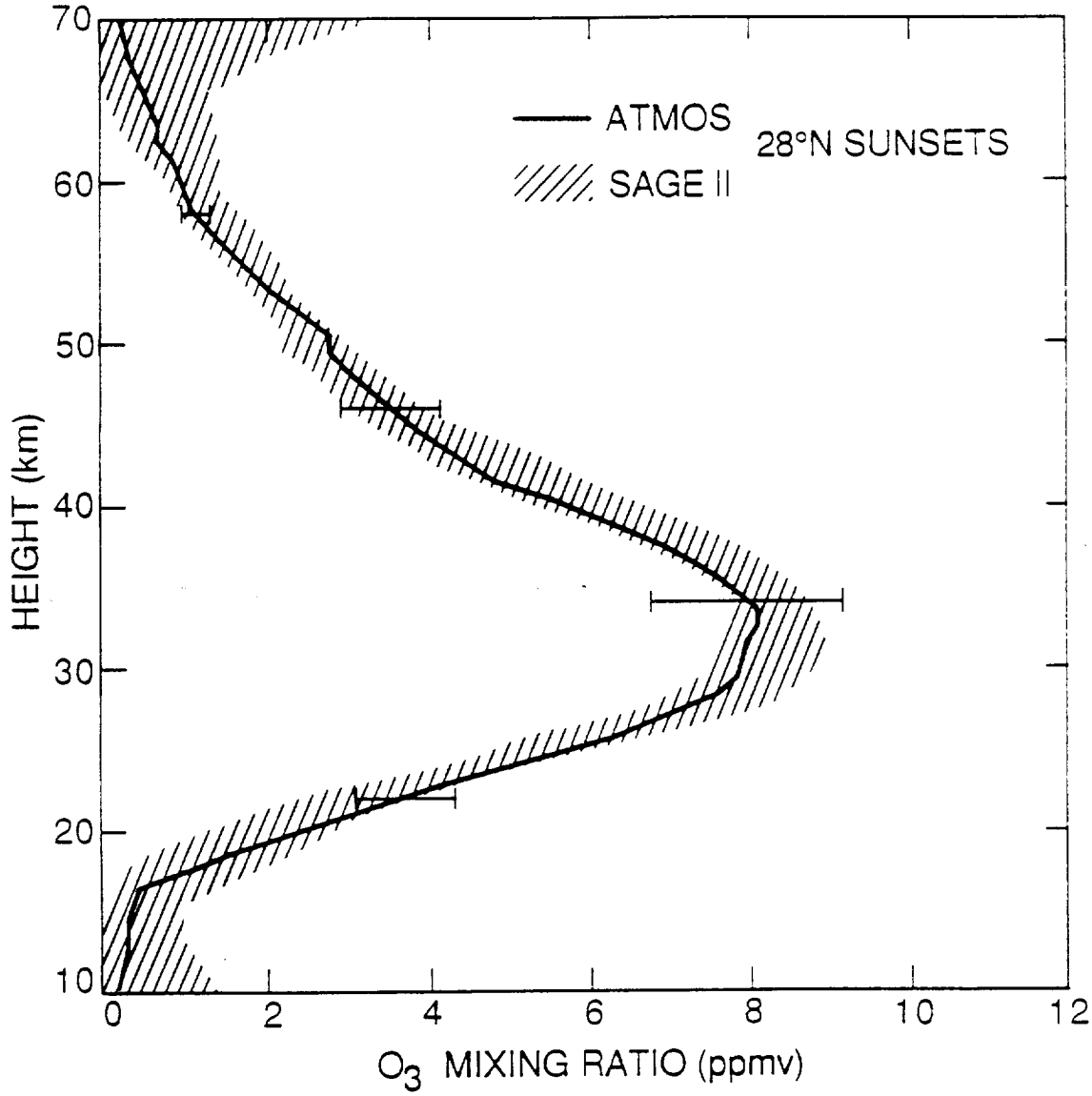

FIGURE 17A

M.R. GUNSON ET AL.

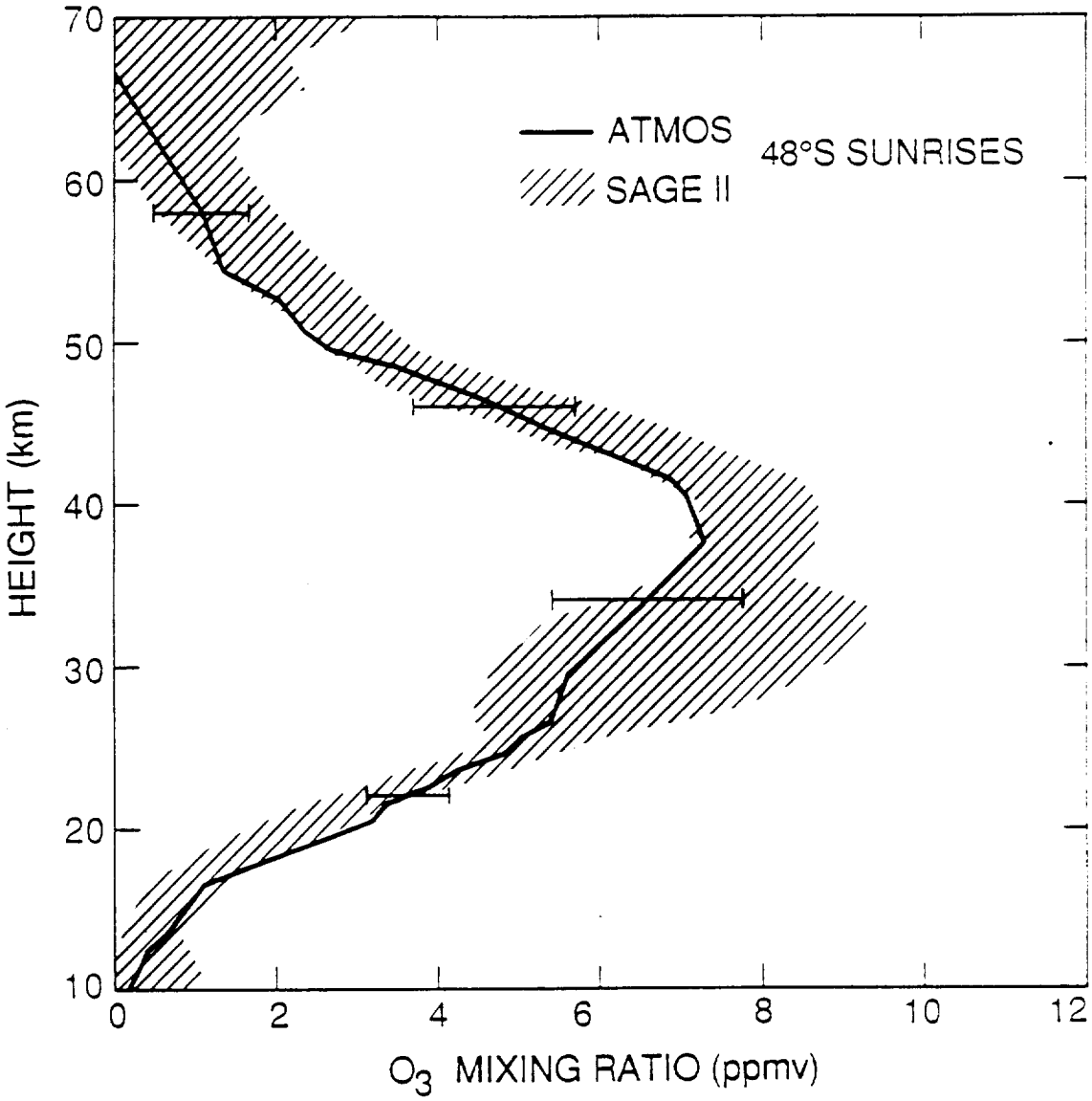

FIGURE 17B

M.R. GUNSON ET AL.

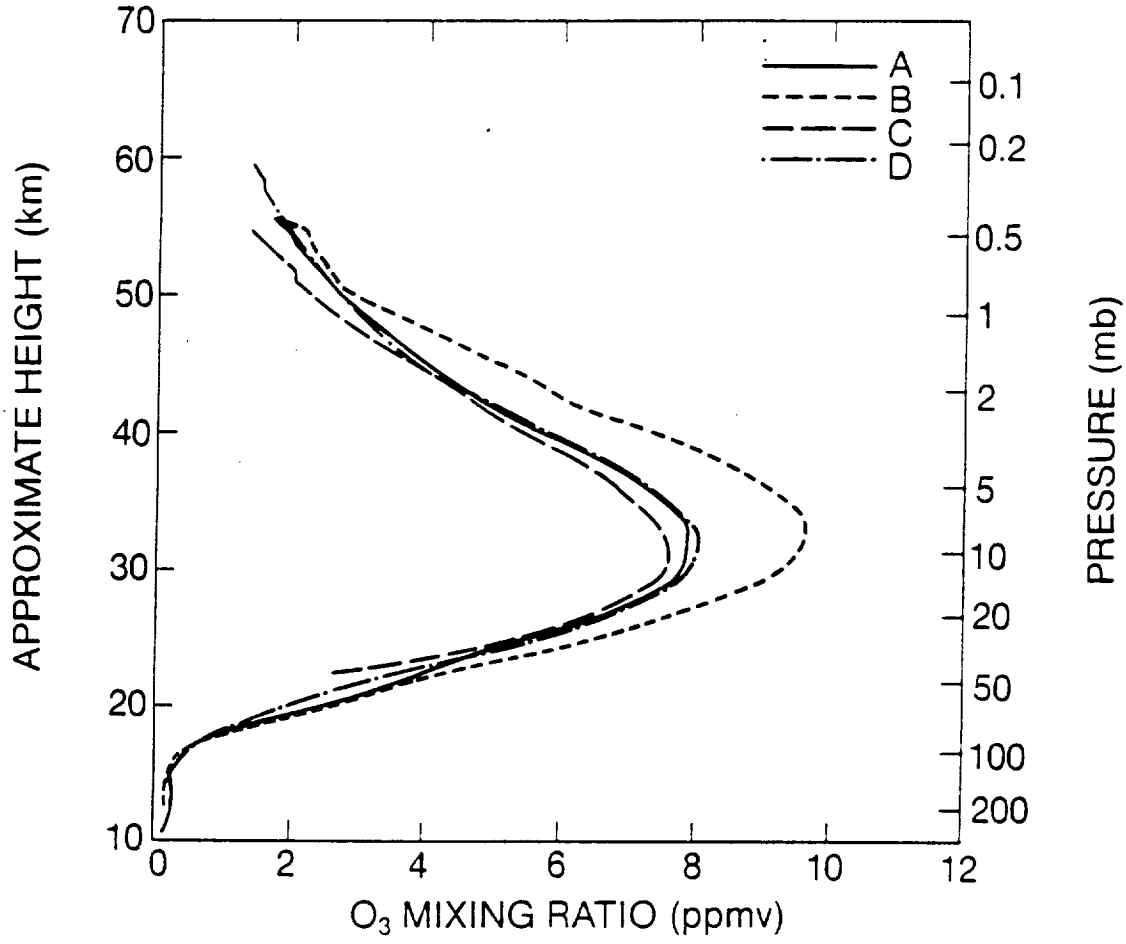

FIGURE 18

M.R. GUNSON ET AL.